

Diplomarbeit

Production Procedures of the Sensor Ladders for the Belle II Silicon Vertex Detector

ausgeführt zum Zwecke der Erlangung des akademischen Grades eines
Diplom Ingenieurs unter der Leitung von

Doz. DI Dr. Christoph Schwanda
Institut für Hochenergiephysik

Betreuer: DI Dr. Thomas Bergauer
Institut für Hochenergiephysik

eingereicht an der Technischen Universität Wien
Fakultät für Physik

von

Stefan Schultschik, B.Sc.

Matrikelnummer: 0825578
Kundmanngasse 4/4
1030 Wien

Wien, am 27. Juni 2015

Kurzfassung

Das Institut für Hochenergiephysik (HEPHY) ist beauftragt, spezielle Komponenten (sogenannte 'L5 Ladders') für den Silizium Streifen Detektor des Belle II Experimentes in Tsukuba, Japan anzufertigen. Die Aufgabe des Silizium Streifen Detektors ist es, geladene Teilchen mikrometergenau zu detektieren. Die Teilchen entstehen am Ort des Zusammenstoßes (dem sogenannten Interaction Point) beider Teilstrahlen. Die L5 Ladders bestehen aus Silizium Sensoren, Ausleseelektronik und einiger anderer Komponenten, welche für die elektrische und mechanische Funktion notwendig sind. Die angestrebte mechanische Genauigkeit einer fertiggestellten L5 Ladder liegt bei weniger als einhundert Mikrometer.

Der Autor dieser Arbeit entwickelt ein vollständiges Konzept für die Produktion der L5 ladders und fertigt anschließend in einem eigens dafür eingerichteten Reinraum ('Module Reinraum') am HEPHY mehrere Prototypen an. Das Konzept beinhaltet den ausführlichen Arbeitsablauf des Produktionsprozesses, inklusive einiger Messungen zur Überprüfung der Genauigkeit und Funktion der Ladder, zwischen einzelnen Schritten. Als Vorbereitung für die Produktion werden notwendige Geräte und Werkzeuge aufgebaut und programmiert. Messmethoden für mechanische Genauigkeitsmessungen werden entwickelt und angewendet. Die Messwerte werden vom Autor analysiert, visualisiert und anschließend mit den Daten der einzelnen Prototypen verglichen.

Jeder Schritt des Produktionsprozesses wird während der Ausführung überwacht um dem Autor die kontinuierliche Verbesserung des Aufbaus und der Prozedur zu ermöglichen. Nach der Fertigstellung eines Prototypen zeigen die Messungen die erreichte mechanische Genauigkeit. Diese Information wird benutzt um weitere Feineinstellungen und Anpassungen vorzunehmen. Eine zunehmende Verbesserung der mechanischen Genauigkeit von Prototyp zu Prototyp kann beobachtet werden (siehe 4.2.3). Die zuletzt gefertigte Ladder weist Abweichungen

der Sensoren von ihrer Nominalposition von weniger als $100\mu m$ auf. Dieser Abweichungen liegen deutlich unter den Toleranzgrenzen und die Prototypenproduktion gilt daher als sehr erfolgreich.

Abstract

The Institute of High Energy Physics (HEPHY) is in charge of building components (so called “L5 ladders”) for the Silicon Vertex Detector of the Belle II experiment in Tsukuba, Japan. It is the successor to the well established Belle detector. This detector tracks charged particles with a precision of a few micrometers in the vicinity of the interaction point and plays a crucial role in the experiment. The L5 ladders consist of silicon sensors (the active part of the detector), front end readout chips and a few other components, necessary for the electric and mechanic function of the ladder. The target mechanical accuracy of the assembly is in the order of a few tens of micrometers.

The author develops a concept for the production of the L5 ladders in HEPHY’s module cleanroom. This involves the design of a work flow chart of the production process with continuous quality control and setting up/programming the tools, devices and machines needed for the production. Different prototypes are built with this setup and measurement methods are developed and applied to verify the mechanical accuracy of the production process. The author analyses, visualizes and compares the measurement data of each prototype with each other.

During the production of the prototypes, each step is closely reviewed. This allows the author to refine the setup and procedures. After the production, the analysis of the measurement data shows information of the achieved mechanical accuracy. This information is used to discover further possibilities of mechanical improvements. By repeating this process, it can be seen that the mechanical accuracy of a ladder is improved each time (see 4.2.3). The latest ladder prototype features mechanical offsets of the silicon sensors of less than $100\mu m$. This is a successful result which is within the limits of the maximum sensor tolerances.

Contents

1	Introduction	1
1.1	The physics of seeing particles	1
1.2	The (Super)KEKB collider	4
1.2.1	Technical aspects	4
1.2.2	The SuperKEKB upgrade	6
1.3	The Belle II detector	7
1.3.1	Detector overview	7
1.3.2	The Belle II upgrade	9
2	The silicon vertex detector (SVD)	11
2.1	Semiconductor physics	11
2.2	Detector layout	13
2.2.1	Ladders	13
2.2.2	Ladder mount	15
3	Concept and SVD ladder design	17
3.1	Setup	17
3.1.1	Overview and status	17
3.1.2	Devices	17
3.1.2.1	Coordinate measuring machine (CMM)	17
3.1.2.2	Wire bonding machine	22
3.1.2.3	Jigs	24
3.1.2.4	Other devices	25
3.1.3	Software	25
3.2	Ladder assembly procedure	27
3.2.1	Work flow chart	27
3.2.2	Assembly	28
3.2.2.1	L5.1 Sensor + flexible PCB assembly	28
3.2.2.2	L5.2 Rib assembly	30
3.2.2.3	L5.3 Flexible PCB assembly part 1	33

3.2.2.4	L5.4 Ladder assembly part 1	36
3.2.2.5	L5.5 Flexible PCB assembly part 2	38
3.2.2.6	L5.6 Ladder assembly part 2	42
3.2.3	After production	45
4	SVD ladder assembly	50
4.1	Building the first prototype	50
4.1.1	Assembly	50
4.1.2	Measurements and evaluation	51
4.2	Further progress	60
4.2.1	Class C prototype	60
4.2.2	Class B prototype	63
4.2.3	Summary and Results	66
5	Outlook	69

1 Introduction

1.1 The physics of seeing particles

To be able to 'see' fundamental particles, they have to be created first. Particles can be produced through conversion of energy into mass. This can be done in a particle collider where two beams of particles are e.g. accelerated in different directions and then being intertwined to create a collision. The particles of each beam will hit particles of the other beam at speeds close to the speed of light. This corresponds to energies in the GeV domain. Those energies enable the creation of fundamental particles while the source particles dissipate. These particles fly away from the collision point into the detector. A second method uses a linear collider, where the accelerated particles hit a fixed target.

Particle accelerators are not only used in fundamental research. In fact, in 2010 roughly 26 000 particle accelerators existed worldwide [11]. Only about 1% of these machines are used for fundamental research. Most other particle accelerators are used for either radiotherapy in medicine or ion implantation in industry. One major difference between medicine and industry accelerators on one hand and research accelerators for high energy physics experiments on the other hand, is the way the accelerated particles are used. While in radiotherapy and ion implantation the particles are focused on a fixed target for a certain amount of time which creates an observable effect in the target, the particles used in fundamental research interact with each other and are used to create new particles. These new particles are then made visible by a particle detector.

Depending on the energy and cross section of the different particles, they will interact differently with certain detectors. The produced particles live either long enough to detect the produced fundamental particles themselves, or they decay into various other particles [24]. At some point, one of the decay products will live long enough to be detected. These decay products are:

1 Introduction

- Hadrons
 - The proton, the neutron, and their anti particles
 - The charged pions
 - The charged kaons and the neutral kaon
- Leptons
 - The electron and the positron
 - The muon and the anti muon
- The photon

By studying the detected particles, whether they are decay products or the original particles, it is possible to reconstruct the chain of events that happened during and after the collision. Two long lived particles, the neutrino and its anti particle the anti neutrino will not interact with the material of the detector enough to be able to detect.

There are different possibilities to 'see' elemental particles. Seeing something in a physical sense, means reflecting light off of its surface and detecting that light. Light that a human eye can detect is in the range of $350 - 750nm$. This is much larger than the dimension of the particles in question. That only leaves the possibility to detect particles by looking at the traces they leave in a detector. These traces are left because of direct interaction of the particles with the material of the detector [5].

Interaction with the material of the detector can be found due to one of the following processes:

- Elastic collision with electrons of an atomic shell
- Elastic collision with a recoiling nucleus
- Emission of radiation through excitation or ionization of electrons in the atomic shell
- Emission of bremsstrahlung due to deviation of charged particles in the Coulomb field of a nucleus

- Emission of γ rays or particles due to excitation of a nucleus through inelastic collision
- Emission of Cerenkov radiation due to fast, charged particles
- Emission of transition radiation of a fast particle between electrical insulators with different resistances

These characteristic processes can be used to detect and categorize fundamental particles [10]. It is clear therefore, that a particle detector is not one large device that determines what particles there are in a bunch, rather that it consists of multiple detectors, each in its own layer around the interaction point, where the particle beams collide. Detectors are distinguished by their main function [6].

There are tracking detectors which produce electrical signals that are generated by particles that travel through it. Several layers of these tracking detectors are used to reconstruct the path of the particles. Usually a magnetic field is used to deflect charged particles. The deflection can be used to gain information about the particles momentum.

Calorimeters use a high density material to absorb the incident particles and measure their kinetic energy. The measurement is done in several layers throughout the Calorimeter. Two kinds of calorimeters can be found in a particle detector. The electromagnetic calorimeter is used for electrons and photons which interact with electrically charged particles in the material of the detector. A hadronic calorimeter is used for particles affected by the strong force, e.g. neutrons and protons.

A third type of detectors are the particle identification detectors which measure the Cerenkov radiation and the transition radiation. The Cerenkov radiation depends on the particles speed. This information combined with its momentum determines the mass and therefore the identity of the particle. The transition radiation depends on the energy of the particles which is used to categorize different particle types.

As seen above, each detector delivers different information about the collision event. The goal is to gain all the necessary information to be able to reconstruct the collision event. This is done by feeding all the information from the detectors

through a complex algorithm and combining the information. Once the data forms a clear picture of what happened, an algorithm searches for particles or particle behavior that does not fit the current theory.

1.2 The (Super)KEKB collider

1.2.1 Technical aspects

The KEKB collider is an electron positron collider with asymmetrical beam energies. It is located in the facilities of the 'High Energy Accelerator Research Organization' (KEK) in Tsukuba, Japan [17]. The collider is built underground in tunnels of the old TRISTAN collider, with a circumference of 3016m. The KEKB was completed in 1998, the first physics experiments started in 1999 [19]. One of its main goals was to investigate the CP violation, therefore it required to achieve a very high luminosity. It has a design luminosity of $1 * 10^{34} cm^{-2} s^{-1}$, which was the highest in its class [22]. After some modifications, the luminosity peaked at $2.108 * 10^{34} cm^{-2} s^{-1}$. Figure 1.1 shows a schematic view of the KEKB collider with the circular storage ring and the linear accelerator.

Due to the high luminosity, the collider is called a B factory. The high energy ring (HER) contains electrons with up to 8 GeV, whereas the low energy ring (LER) contains positrons with up to 3.5 GeV. As mentioned above, the collider uses asymmetrical beam energies with which it produces collisions with a center of mass energy of 10.58 GeV. This is the optimal energy to produce $B\bar{B}$ meson pairs through the Y(4s) resonance. For the lower resonances Y(1s), Y(2s) and Y(3s) it is energetically not possible to produce $B\bar{B}$ pairs. It can also run the Y(5s) and Y(6s) resonances [25]. The asymmetric beam energies create a boost of the colliding particles in the direction of the HER. This enables the detection of particles with a short lifetime, which would otherwise decay before they would hit the detector.

The electrons and positrons are accelerated with a linear collider (LINAC). The acceleration in the LINAC is done in eight sections by a total of 54 acceleration modules which each produce an energy gain of 160 MeV. The maximum theoretical energy gain is therefore 8.6 GeV. An acceleration module uses a high power RF signal to collect the electrons into bunches and accelerate them [23].

The electrons which are accelerated to 8 GeV, are emitted from a photo cathode RF gun which produces an electron bunch charge of 1 nC. The electrons for positron production are emitted from an electron gun using an electric field of 200 kV acceleration voltage [19]. These electrons are accelerated in the first half of the LINAC to 3.7 GeV. At this energy, they will hit a Tungsten [2] plate which produces positrons of 1 nC per bunch through pair production. The electrons are deflected in the field of the Tungsten nuclei and emit bremsstrahlung [26]. If the energy of the photon is more than double that of the rest energy of an electron, e^-e^+ pair production in the field of a nucleus (to transfer some of the momentum to it) is possible. At energies above 3 MeV pair production is the dominant process. In the second step the positrons are separated from the electrons and accelerated to their full energies of 3.5 GeV in the second half of the LINAC.

At the end of the linear collider the electron and positron bunches are injected into the 3016 m long synchrotron storage ring. One bunch of electrons contains about $1.4 * 10^{10}$ particles, while a bunch of positrons contains about $3.3 * 10^{10}$ particles. A bunch of particles is roughly 4 mm long and separated from the following bunch by about 59 cm, which corresponds to a separation time of about 2 ns [22, 19].

This storage ring consists of two evacuated beam pipes in which the electrons and positrons circulate. To keep up the circular motion, the particles need to be deflected. This is done with bending magnets outside of the beam pipe. These bending magnets are not spread across the storage ring, but are located in several sections of the ring. Therefore, the particles travel not in a perfect circular motion. After a bending section, they travel in a straight line to the next bending section. Bending the particles causes them to lose energy and slow down. Typical loss energies per turn are in the area of 2 MeV. Therefore, an acceleration region, the so called RF cavities, are built into one of the straight sections, which accelerates the particles by the amount of the lost deflection energy, but not more. Both, the electrons and positrons can be accelerated simultaneously in different beam pipes due to their opposite charge and their opposite flying direction [10].

The storage ring also allows to increase the number of particles per bunch by injecting them in the correct moment with the LINAC into the passing particle bunch. The key task of the storage ring is to bring particle bunches of each sort in the same time into a specific region where they can collide. This is called the interaction region, which geographically lies in the Tsukuba experimental hall.

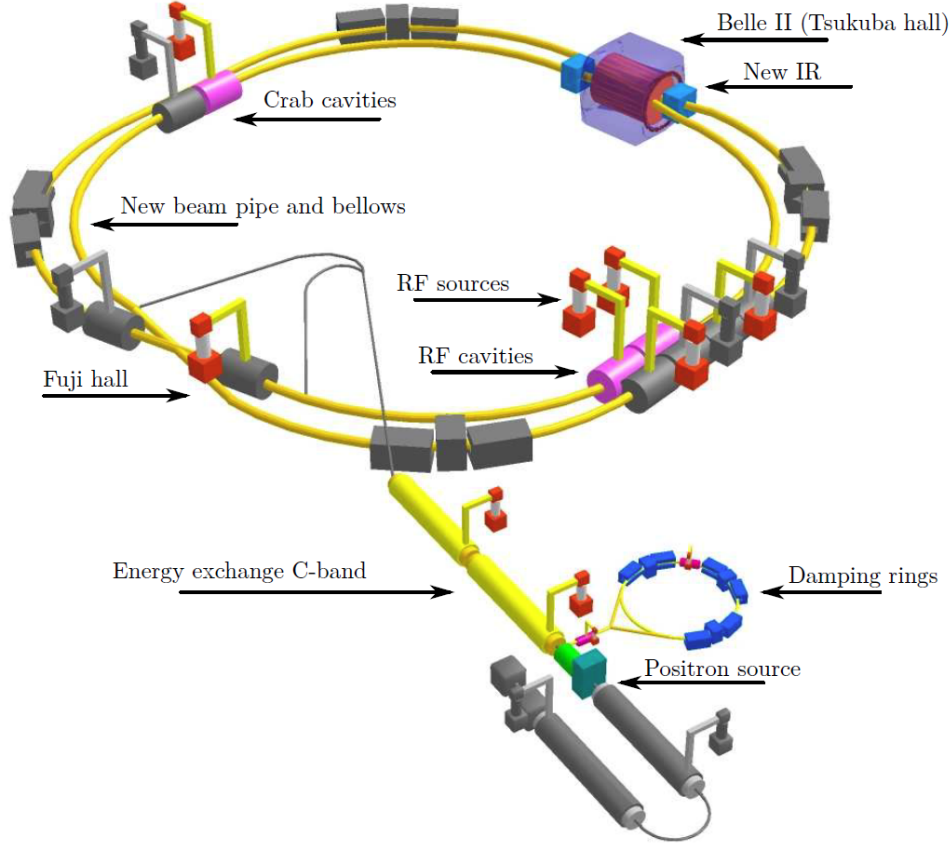


Figure 1.1: KEKB collider in Tsukuba with upgrades to SuperKEKB, Japan [23]

All around the interaction region, the particle detectors are placed. The particles are guided to the interaction region via electromagnetic lenses. They are focused to an interaction point so that there, the current density during a collision is maximized. The rate N at which collisions between e^- and e^+ occur is calculated by the number of particles N_1 and N_2 per bunch, the diameter A of the beam, the cross section σ and the number of bunches per time f

$$N = \int_0^t \frac{N_1 * N_2}{A} * f * \sigma dt = \int_0^t L * \sigma dt$$

whereas L is called the Luminosity of the storage ring. It is therefore a factor corresponding to the number of produced particles per collision.

1.2.2 The SuperKEKB upgrade

The KEKB collider was in service from 1998 until 2010. It was shut down because the associated Belle experiment has successfully run its course and a major

upgrade of both the collider and the detectors were planned. This upgrade from KEKB to SuperKEKB is going on right now and the commissioning phase will start in 2017. The primary upgrade plans concern the increase in luminosity of the collider to a design value of $8 * 10^{35} cm^{-2} s^{-1}$ which is 40 times more compared to the KEKB [19]. This will produce much more useful particle decays in a given time frame. To achieve this goal, crucial collider parameters and parts will be changed or renewed. The plans to increase the luminosity involves a higher beam current and better focusing of the beams in the interaction region. The beam current will be increased from 1.6A / 1.2A in the LER / HER to 3.6A / 2.6A. This increases the total number of colliding particles. The beam energy asymmetry will also be reduced to 7 GeV in the HER and 4 GeV in the LER. To focus the beams, the Nano-Beam scheme has been introduced (see figure 1.2) [22]. Unlike the KEKB, which used head on collisions, this scheme uses a large crossing angle of 83 mrad and a small beam size to further increase the luminosity. This means, the beams are squeezed to narrower bunches by a stronger magnetic field. Therefore more particles are squeezed into the overlapping region.

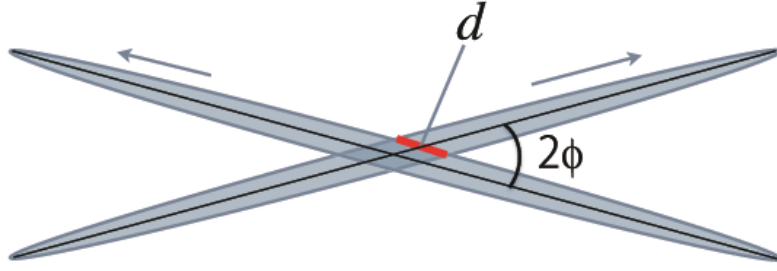


Figure 1.2: Schematic drawing of the Nano-beam scheme [2]

The Beta function β^* , which gives the distance between the focus point and the point where the beam is twice as wide, will be reduced by a factor of 20 [12].

1.3 The Belle II detector

1.3.1 Detector overview

The Belle detector is a general purpose 4π detector which is used to find, track and identify particles that are produced during the beam collisions. It sits in the area around the interaction region in the Tsukuba Hall. In the recent decade, the Belle detector made a name for itself by its high vertex resolution and broad

1 Introduction

measurement spectrum. The detector was not only used for one experiment, but it was used for many other research topics, such as charm physics, tau lepton physics, hadron spectroscopy and two photon physics [7]. One of the most important physical accomplishments was the observation of the existence of a third family of quarks and the observation of CP violation in the B meson system. The former was a result which was theoretically proposed in 1972 by Makoto Kobayashi and Toshihide Maskawa [20]. They received the Nobel Prize for Physics in 2008 for their work.

The Belle detector consists of several different detectors, each designed for a different measurement. All three detector types, tracking detectors, calorimeters and particle identification detectors can be found in the Belle detector. The tracking detectors sit in the innermost area near the interaction point because the particles decay so rapidly, that most of them are not able to reach the detector, only their decay products. The job of these tracking detectors is to track the flight path of the particles to be able to reconstruct the events that happened at the interaction point. The more spacious detectors, such as the calorimeters and particle identification detectors are installed outwards. The fact that the collider uses asymmetrical beam energies, means that most of the center-of-mass system will travel in the direction of the 7 GeV electrons. The detectors are specially designed to account for that by covering a polar angle from 17° to 150° .

The different detectors that Belle consists of are [9] [24]:

- Silicon Vertex Detector (SVD): Four layers of double sided silicon microstrip sensors to track the decay particles of the B mesons
- Central Drift Chamber (CDC): A large gaseous detector with drift cells which measures the tracks and momenta of the decay products
- Silica Aerogel Cherenkov Counter (ACC): Used for particle identification, mainly to distinguish between pions and kaons
- Time of Flight Counter (TOF): It uses TOF and trigger scintillation counters (TSC) to measure the particles' velocities, which gives information about their identity
- Electromagnetic Calorimeter (ECL): Detects high energy photons in the full Belle angular region using an array of crystals with photodiodes and

measures their energy and position

- Kaon and Muon Detection System (KLM): Detects muons and kaons, and distinguishes between them, using alternating layers of glass electrode resistive plate counters and iron plates
- Superconducting Solenoid: Provides a homogeneous magnetic field of 1.5T along the beam axis

These parts assembled together create the complete Belle detector.

1.3.2 The Belle II upgrade

The upgrade of the KEKB collider to the SuperKEKB collider comes along with a major upgrade of the Belle detector as well. The detector has to be adjusted to the new parameters of the collider, and new parts coming from years of research and development will increase the accuracy of the detection process. The components for Belle II are currently being developed and produced. Assembly of the Belle II detector will start in Q2 2016, after the collider in that area is finished. Figure 1.3 shows the Belle II detector in the top half and the old Belle detector in the bottom half.

The main upgrades of the Belle detector will include [2]:

- The silicon vertex detector SVD will be extended by 2 layers of a silicon pixel detector PXD, based on the DEPFET (Depleted P channel Field Effect Transistor) technology on the inside and four layers of a larger diameter SVD on the outside. This will increase the 2D vertexing capability.
- The readout time will be drastically reduced by introducing the APV25 chips compared to the current VA1TA chips.
- The new CDC will get smaller drift cells and extend to a larger radius.
- The particle identification devices will be upgraded to a more compact size with an even higher performance and faster readout electronics.
- The ECL upgrade includes the replacement of the complete electronics to a faster and more radiation tolerant version.

1 Introduction

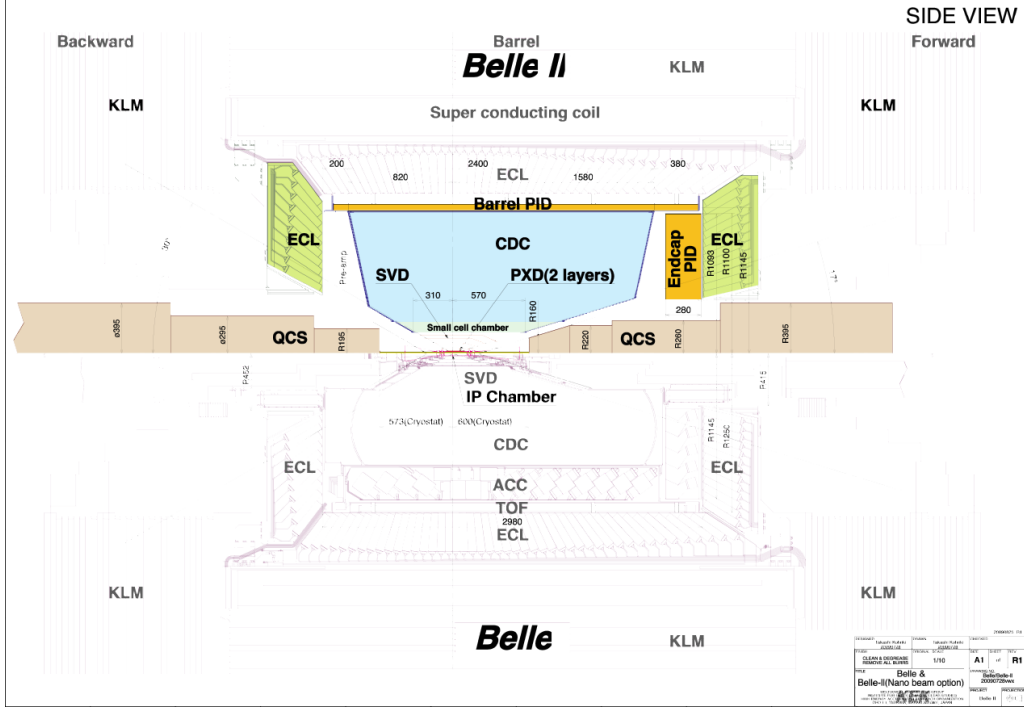


Figure 1.3: Top half: Upgraded Belle II detector, Bottom half: former Belle detector [2]

- The endcap part of the KLM detector is replaced with silicon photomultiplier instrumented scintillators.
- The new data acquisition system DAQ meets the requirements of the considerable higher event rates.

Figure 1.3 shows the Belle II detector compared to the former Belle detector. These upgrades will improve the performance of the detector in several aspects:

- The vertex resolution will be improved by the excellent spatial resolution of the two innermost pixel detector layers.
- The efficiency for reconstructing K_S decays to two charged pions with hits in the SVD is improved due to its larger volume.
- The new particle identification devices in the barrel and endcap regions extend the very good pion/kaon separation to the kinematic limits of the experiment
- The new ECL electronics will considerably reduce the noise pile up, which is important for missing energy studies.

2 The silicon vertex detector (SVD)

2.1 Semiconductor physics

¹ Semiconductor detectors are used for a variety of different appliances, e.g. for industrial applications such as medicine or security, in nuclear physics, e.g. for energy measurements of charged particles or in particle physics for tracking particles and decay vertices. These are only the most important appliances, but there are many more.

The sensors of the Belle II semiconductor detector are made out of silicon. The main reason for this material is that it can be operated under room temperature. In comparison, other detector materials such as e.g. germanium, have to be cooled with liquid nitrogen during operation because of its small band gap.

Another very important parameter is the Signal to noise ratio (SNR) which is a factor that describes how well a signal can be interpreted over the electronic noise. A large SNR requires a large signal and a low noise level. With silicon detectors, the number of thermally created e^-h^+ pairs is four orders of magnitude larger than the signal. Using doped silicon where charge carriers are removed solves this problem [4].

The task of a semiconductor detector is to measure e^-h^+ pairs that occur when charged particles, with at least twice the rest energy of an electron, hit the material of the detector. A reverse bias voltage of 80 – 120V is applied to every sensor. This is done to fully deplete the sensors, creating a depletion zone across the whole sensor area. The electrons and holes travel in different directions and using the previously etched metalized strips, the drift current creates electrical signals which are then transferred to the front end read out electronics (see figure 2.1).

¹Small parts of the section 2.1 are reused or adopted from the authors earlier work [28]

2 The silicon vertex detector (SVD)

Using high frequency wire bonding the strips are electrically connected to flexible PCB's. They are made of Kapton foil which holds thin electronic strips. They are glued onto the silicon and bent around it. There, additional wire bonds create the connection to the readout electronics. A total of roughly 13 000 wire bonds are necessary for one ladder.

A basic property of semiconductor detectors is that they have a high mass density. This means that the particles traveling through this material will lose a lot of energy over a short distance. This energy loss can have several reasons, see section 1.1. The energy necessary to ionize silicon atoms is 3.6 eV.

The production of silicon sensors is done on an industrialized scale. During the so called planar process, different techniques are used to prepare the silicon semiconductor to be used as a detector. The n doped silicon is heated up in a furnace in order to create a thermal oxide layer on top of the silicon. Then, by using photolithographic techniques, this oxide layer is etched off at certain areas e.g. to form strips. Further doping, metalization and etching steps are necessary to create the silicon semiconductor detector [21]. In case of the Belle II SVD, these steps are performed on both sides of the silicon, for higher accuracy and less material inside the particle path.

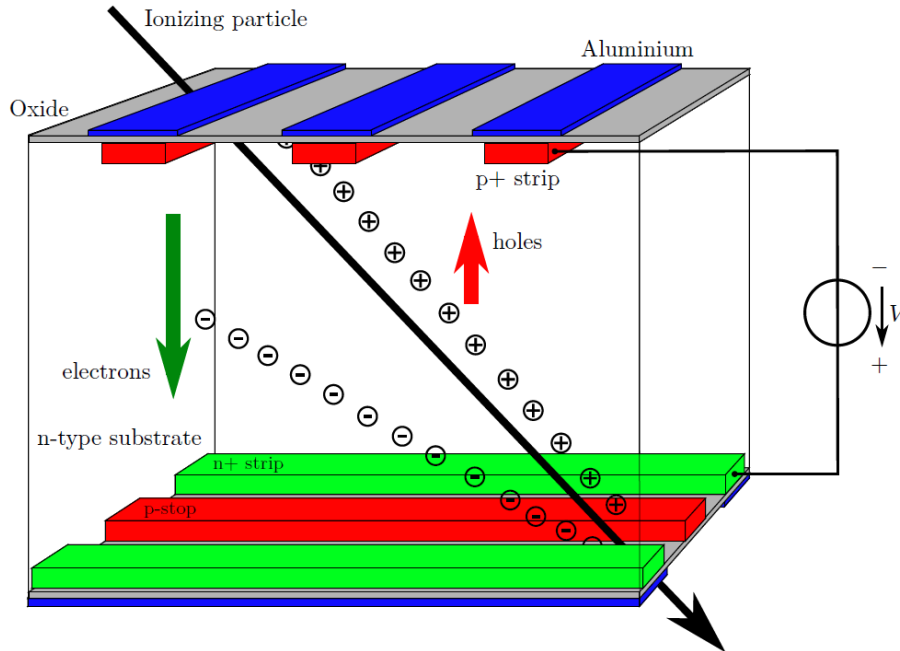


Figure 2.1: Schematic drawing of the working principle of a semiconductor detector [24]

2.2 Detector layout

2.2.1 Ladders

The Belle II detector consists of six layers of detector modules. These six layers are divided into four outer layers of double sided silicon sensors and two inner layers of DEPFET pixel sensors. Therefore, only layer three through layer six are silicon strip detectors. The layers are surrounding the interaction point. This means that they are placed concentrically around it. Several modules are used for this with increasing numbers of sensors on each layer. Layer five, which is built at HEPHY uses four silicon sensor on each module. These modules are the so called ladders. In total, 14 L5 ladders will be needed to build the layer five of the vertex detector. Including prototypes and spares, up to 22 ladders will be built.

The L5 ladder consists of three rectangular silicon sensors and one trapezoidal sensor. As the beam energies of the SuperKEKB collider are asymmetrical, the majority of particles will fly in one direction. This is the so called forward direction of the detector. This means that there is a need to detect particles in the forward direction more closer to the middle of the detector. This is done by tilting the sensor on the forward side. The tilting angle is nominally 16° . The trapezoidal sensor is therefore placed on the forward position with the short width pointing to the middle of the detector (see figure 2.2). The sensors of layer five are from left to right called: forward sensor ('FWD'), CE sensor ('CE'), -Z sensor ('-Z') and Backward sensor ('BWD'). The assembly of a ladder can be seen in section 3.2.

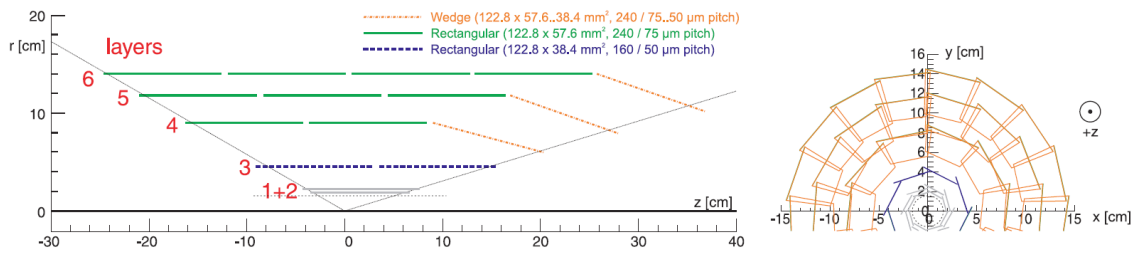


Figure 2.2: Outline of the six layers of the Belle II silicon vertex detector [8]

The supporting structure is made out of carbon fiber material for stability and durability and 'Airex', which acts as a lightweight filler material. These structures are so called ribs. There are two ribs on each ladder for stability which are both

2 The silicon vertex detector (SVD)

connected together on both ends to a mounting structure with which the ladder will be fixed to the detector. The mounting structure on the slanted side is fixed to a prism rail which allows for thermal expansion and contraction without adding tension to the ladder. On top of the ribs are the silicon sensors which are glued onto protruding edges of the ribs.

To connect the sensors' read out strips to the electronics, flexible PCB's are glued on top of the sensors. They connect the sensors to the electronics. In this case, the electronics are glued on top of the flexible PCB's and a connector on one side outputs the signals. The forward and backward sensors are connected via flexible PCB's glued on top of the sensors to separate PCB's with the read out electronics. Between the flexible PCB's and the sensors is a thermal insulating layer of 'Airex' material to thermally and electrically insulate the two. Figure 2.3 shows the parts of which an L5 ladder is made out of.

Ladders of different quality classes are built for different purposes. Class D ladders are electrically non functioning and even have mechanical flaws, e.g. they are built without some of the jigs and procedures used. A class D ladder can therefore only be used to test some procedures and jigs, but it gives only little information on mechanical accuracy. A class C ladder also uses electrically non functioning sensors, but the procedures and jigs used to build the ladders are supposed to be final. Small changes or adjustments are still made. The class C ladder is therefore made to test all the procedures and jigs used in the assembly. The mechanical accuracy on these ladders is final.

A class B ladder uses electrically functioning sensors with small known defects. The ladder is working in the same way a class A ladder would work. The jigs and procedures to build a class B ladder are finalized and the mechanical accuracy is close to the nominal values. The ladder is mainly used to conduct electrical tests. The class A ladders are the ones used in the Belle II detector. The highest mechanical accuracy is expected and only very well working sensors are used. No further tests of procedures or jigs are done using this ladder.

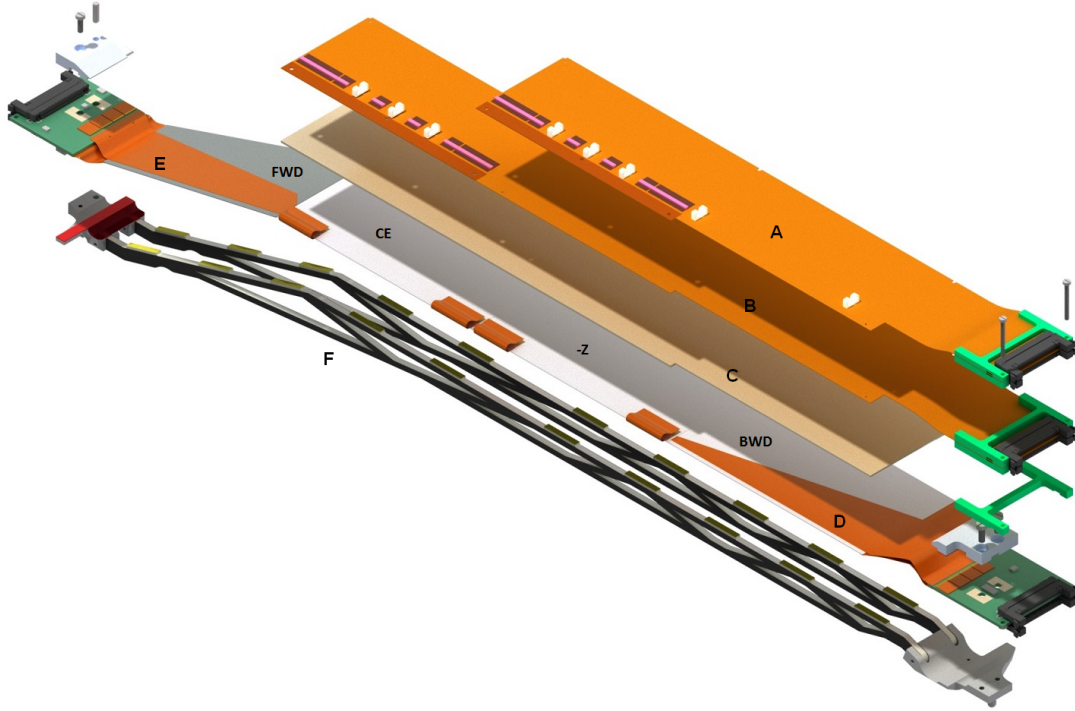


Figure 2.3: Explosion view of the L5 ladder. (A) flexible PCB for -Z sensor, (B) flexible PCB for CE sensor, (C) Thermal insulator sheet, (D) backward sensor with flexible PCB connected to a read out PCB, (E) forward sensor with flexible PCB connected to a read out PCB, (F) carbon fiber ribs with protruding edges on top [7]

2.2.2 Ladder mount

The finished ladders will be mounted to an aluminum supporting frame in a wind-mill structure. They are held by two so called Kokeshi pins which have an indentation to fix them to the aluminum. The ladders are arranged in a way that they are very close to each other, so that the space inside the barrel is best utilized. The ladders, especially the sensors of different ladders, can never touch each other. Mechanical tension would quickly damage the ladders. A test was carried out where the gravitational sag of a ladder was measured. The result was that there was no measurable bending of the ladder to support the theory of this concern.

The aluminum structure, with the slanted part on the right side of it, can be seen in 2.4. It is made in a way that there is as little matter inside the interaction region as possible. Each ladder carries a cooling pipe on top of it to cool down the electronic chips to reduce the noise. The pipe is clipped into cooling clips which are glued onto the flexible PCB's. The thermal contact is provided with a Keratherm material, which is applied to the chips beforehand. The cooling medium is CO_2 .

2 The silicon vertex detector (SVD)

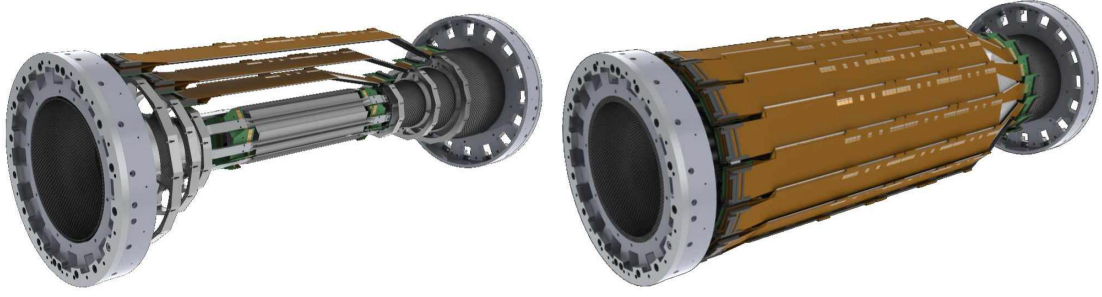


Figure 2.4: CAD drawing of the aluminium supporting frame. (left) One ladder per layer mounted to the frame. (right) Finished Belle II detector with all ladders mounted to the frame [7]

There are only two pipes for each layer. One cooling pipe is wrapped around one half of the ladders on one side of the detector.

3 Concept and SVD ladder design

3.1 Setup

3.1.1 Overview and status

Building a silicon vertex detector requires skill, knowledge and a lot of time. Each part has to be designed and built with almost countless considerations of factors concerning all parameters around it. The foremost concern during the production of the detector will be the accuracy and precision. Even the best sensors won't work properly if they are in the wrong position. This means, special devices, tools and methods will have to be applied to make sure that the final ladders will be as good as it can be.

The Ladders will be built in a cleanroom of the Institute for High Energy Physics in Vienna. This cleanroom offers all the necessary machines to build, measure and test the ladders. During the production, a coordinate measuring machine (CMM), a wire bonding machine, different microscopes and several HEPHY made tools are used. This setup will be used as a basis to develop methods and techniques necessary to build the ladders.

3.1.2 Devices

3.1.2.1 Coordinate measuring machine (CMM)

¹ A coordinate measuring machine is a very accurate device for measuring the geometry of small and large objects. These machines always consist of the same components. Three or more axes can drive the probing head into position. Using a length measuring system, the position of the measuring head is sent to the

¹Small parts of the subsection 3.1.2.1 are adopted from the authors earlier work [28]

3 Concept and SVD ladder design

control computer. The achievable measuring uncertainty is defined through the precision of guidances, bearings, drivetrains, but majorly through the accuracy of the length measuring system of the moving axes. The linearity of the guide way and the rectangularity of two guidances together are highly influential for the mechanical accuracy of the coordinate measuring machine. The guidances are made of hard rock, e.g. Granite which is cushioned on an air bearing. These hard rock guidances have no slip stick effect, are vibration damping and are able to pick up great weight. The drivetrain has the requirement to be robust under constantly changing driving directions and driving velocities [1].

The length measuring system is the crucial component for the accuracy of the coordinate measuring machine. The resolution has to be at least 10 times more accurate than the length measuring uncertainty of the coordinate measuring machine. Usually incremental length measuring systems with electronic data acquisition are used. One basic principle uses optical interferometry which generates a signal using projected light (see figure 3.1). Two very fine scale gratings with equal periods are moved relative to each other [15]. Light passes through the moving scale grating constantly and is diffracted on the back side. The index grating is mounted behind the moving grating. It consists of a surface with highly reflective stripes, usually $0.2 \mu\text{m}$ in height and $2 \mu\text{m}$ apart from each other. The incident light is modulated because of the moving grating. Only if the gaps align, the incident light can pass through. No light can pass through when the lines of one grating coincide with the gaps on the other grating. Photoelectric diodes convert these varying light intensities into electrical signals. The gratings are produced and mounted to create an almost perfect sinus signal. The signal has almost no harmonic content and can be highly interpolated [14].

The Mitutoyo Euro Apex C776 coordinate measuring machine is used for the ladder production (see figure 4.2). It offers a working area of $705 \times 705 \text{mm}$ in X- and Y- and 605mm in Z- direction. Its maximum permissible measuring error MPE_E is $\frac{1.7+0.4 \cdot L}{100} \mu\text{m}$. This means that by measuring a length of 1mm , a maximum measuring error of

$$MPE_E(1\text{mm}) = \frac{1.7 + 0.4 \cdot 1000}{100} \mu\text{m} = 5.7 \mu\text{m}$$

is permissible. The coordinate measuring machine uses 3 driving modes with a maximum driving speed of 520mm/s and a minimal driving speed of $30 \mu\text{m/s}$.

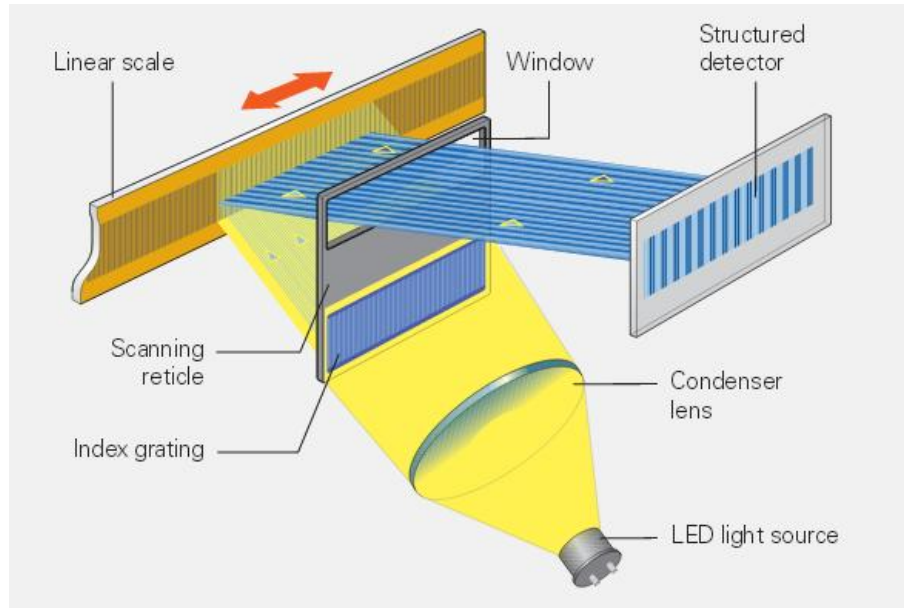


Figure 3.1: Interference measurement principle [15]

The Mitutoyo coordinate measuring machine offers a quick mounting mechanism to switch between probing heads in less than a minute. These probing heads include a tactile sensor to touch probes and an optical sensor to focus on a specific point. The tactile sensor is used primarily to measure surfaces or heights whereas the optical sensor is used primarily to custom coordinate systems. Other sensors include scanning sensors which are dragged across a surface and periodically take measurements of the surface. Using a scanning sensor is usually more accurate and a faster way of measuring a surface. Another method is the non contact scanning sensor. It consists of a high speed laser or a white light source that is projected onto the surface that is measured [19]. By the time the light travels to the surface and back, the position and size of each point can be measured. Even a 3D image can be made. These non contact sensors are used primarily in situations where the sample is made from very soft or delicate material.

The tactile sensor is the most common sensor when using a coordinate measuring machine. It is attached by fixing it in a tight fitting circular guidance. This means it can be rotated in 360° . The machine drives the sensor to a surface point and touches the surface with the tip of the sensor. The tip consists of a ruby ball attached to a stainless steel rod (see figure 3.2).

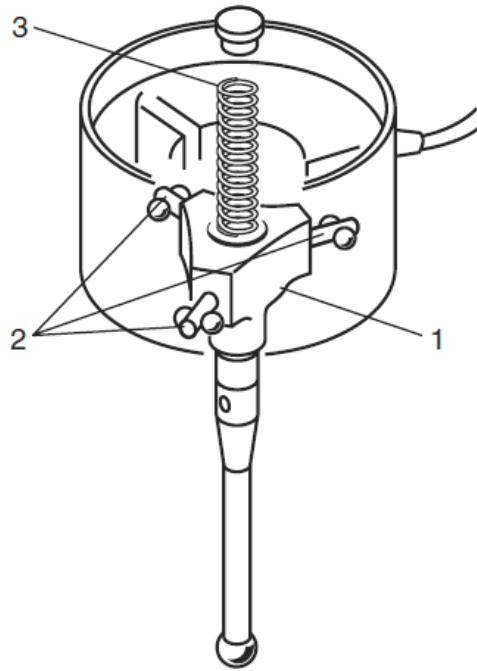


Figure 3.2: Schematic view of the working principle of a high precision tactile sensor; (1) pivotal plate with attached steel rod, (2) spring loaded bearing points, (3) Spring [27]

The working principle of the tactile sensor is based on a change in an electric circuit due to the moving rod [20]. A pivotal plate held in place by a helical compression spring is attached to three spring loaded bearing points. These bearing points consist of ball bearings and a cylindrical roller. The bearing points and the roller act as a closed electrical circuit. When a surface point is touched, the steel rod moves the pivotal plate in a way that one of the electrical contacts open up. This causes a signal to be sent to the controller to take the measurement and move the sensor off the surface again. The force applied to the rod while touching the surface is, in case of the Renishaw PH1, in the order of 0.01 to 0.6N, depending on the mounting position of the sensor. A higher force is needed if the sensor is positioned vertically. The accuracy of the sensor can be improved by mounting it diagonally. The force to move the rod needed is much smaller, by a factor of up to 60.

As an alternative to the tactile sensor, an optical sensor can be used for surface measurements. In the case at HEPHY this sensor consists of a camera that transfers live images to the computer screen, a laser to find positions on the surface

more easily and an external light source to increase the brightness of the images. The laser is used as a guiding system on the surface. It points directly in the middle of the focal length of the camera. The focal length is 4.5 cm above the surface. The camera images are not analyzed by software, but by the operator. Other optical sensors include triangulation sensors, image interpreting sensors or interferometers.

With the help of the camera, the coordinate measuring machine can be used as a gluing robot as seen in 3.3. The camera focuses on several markers on the surface and the software aligns a local coordinate system which is used during gluing. A glue dispenser is mounted near the camera and attached to a glue dispenser. The glue dispenser can be automatically operated by the software, starting and stopping the flow of glue. This is done by compressed air that pushes the glue through the needle. The camera is used only for the alignment process. The following movements of the coordinate measuring machine are controlled automatically by software.

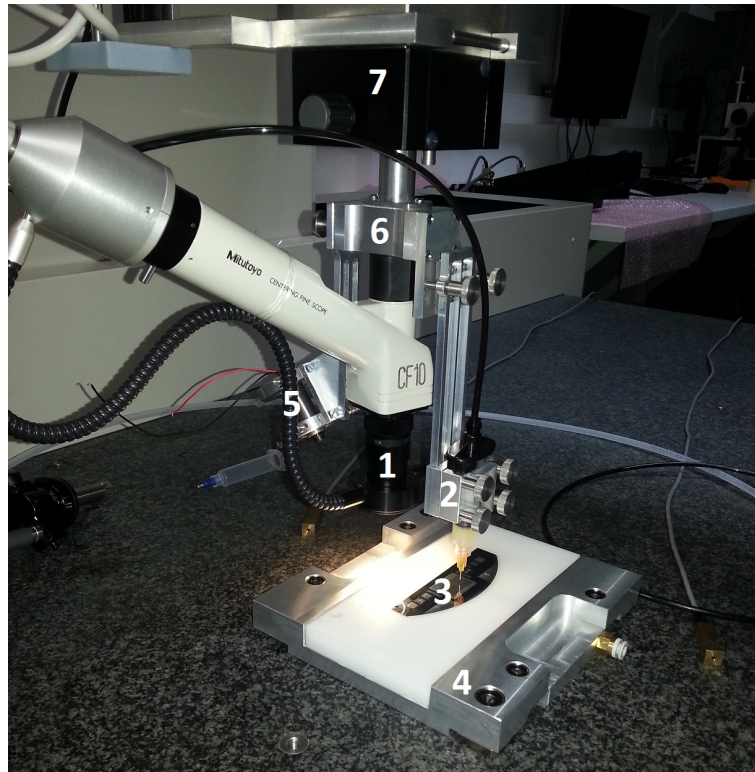


Figure 3.3: CMM with adjustments for use as a gluing robot. (1) Camera with additional lighting, (2) holder for gluing needle with needle attached, (3) test sample for gluing, (4) gluing jig, (5) Laser for guidance, (6) Mounting head for gluing holder and camera, (7) CMM mounting head

3.1.2.2 Wire bonding machine

A wire bonding machine is used to create electrical connections. One advantage of doing this with a large wire bonding machine is to be able to make connections using wires with a tiny diameter (10 to 1000+ μm). Several consecutive connections can be made each second. The wire does not even need to be round, as rectangular ribbon forms are possible.

A wire bonding machine consists of four main components. The power supply converts the frequency of the mains electricity to a high frequency signal (20 – 40kHz). This is the frequency that will be applied to the wire later. In the next step, the converter (transducer) receives this electrical signal and directs it to piezoelectric discs. These will start to expand and contract at the same ultrasonic frequency. Therefore, they convert the electric energy into mechanical vibratory energy. The vibration energy is transmitted through an amplitude modifier where the amplitude of the sound wave is increased. The fourth component is the so called sonotrode, which will transfer the vibration energy to the wire. The sonotrode also pushes down the wire to the pad. The wire will start to vibrate with the given ultrasonic frequency. In the bonding area, the vibration energy is converted to heat, due to friction between the wire and the pad. The temperature rises until the two materials start to melt. Once the whole bonding area is melted, the sonotrode will release the pressure and wait until the bond is cooled of and the two components are welded together [18].

The bond between the wire and a bonding pad is formed by bringing the wire in contact with the other material and applying thermal or mechanical energy. Three types of bonds can be formed [13]:

- Intermetallic compounds
- Diffusion bonds
- Atomic welding

The intermetallic compound bonding, also called thermosonic bonding method is done with the ball bonding technique. It has the advantage that it can be used for gold, copper, aluminum and other similar types of materials. The bond forms in a small layers between the wire and the pad when both atom types react with each

other and inter diffuse. These layers are called Inter Metallic compounds (IMC) [13].

Diffusion bonding [13], also called thermocompression bonding works by placing the wire on the pad and applying heat and a high pressure. Atoms from the wire will diffuse into the pad and vice versa until no clear boundary layer exists anymore.

Atomic welding, also called ultrasonic bonding is a method where a high ultrasonic frequency (typically 100-200 kHz) is applied to the wire as it touches down on the pad. The friction causes the wire and the pad material to heat up and weld together. As the welding point cools, the joint strength will be close to the strength of the parent material. This method is bonded with the wedge bonding technique [18].

The ultrasonic bond, which is used at HEPHY, can be made by two different bonding techniques, either Ball bonding or Wedge bonding. The technique is depended on the materials used. Wedge bonding has the advantage that it can be used with an aluminum wire, without the need to apply additional heat. The wire is molten together with the pad by only applying ultrasonic energy and little pressure. This, and the fact that no protective gas atmosphere has to be supplied, makes the wedge bonding technique particularly interesting for smaller and non industrialized settings, such as HEPHY.

In case of the wire bonding machine used during the production of the ladders, a Delvotek G5 wedge wire bonding machine was chosen. The machine can create several ultrasonic bonds each second while still leaving versatile options to program and operate it. The wire is a AlSi 1% aluminum wire with a diameter of $25\mu\text{m}$. The pad material on the Sensor is also aluminum. This means, that a melting temperature of 660°C has to be induced by the ultrasonic vibrations and pressure onto the wire [16]. The bonding pads on the flexible PCB's however are a stacked system of different materials. The ground material is copper. The complete wiring of it is also copper and directly connected to these pads. The middle part of the stacked system is a $3 - 5\mu\text{m}$ thin Nickel layer, which is used to weld the wire together. As a protective layer against corrosion, a $1\mu\text{m}$ thin layer of gold is attached on top.

3 Concept and SVD ladder design

The melting temperature to bond the AlSi 1% wire to the Ni pad is 1455°C [3]. The additional heat compared to the the pure aluminum bonds is provided by a combination of higher amplitude of the ultrasonic vibrations and pressure applied. The frequency during bonding is set to a fixed value of 65.840 kHz. To achieve the highest bonding strength, a row of bonds is prepared, each bond made with a different vibration amplitude and different pressure. The pressure is set to $10-30\text{g}$, while the ultrasonic power is set as a percentage of the maximum achievable power of $P = U_{PP} * I = 0.08\text{V} * 0.04\text{A} = 3.2\text{mW}$ according to the handbook. This power and pressure is applied to a bonding area of roughly $30 \times 80 \mu\text{m}$ and is enough to create the melting temperatures needed. The bonding time is treated as a constant.

For testing of the reliability of the bond process and the correct parameters a so called pull-tester is used. This device uses a small hook to pull the bonds off of the pads and measures the required force while doing so. The maximum bonding strength measured, corresponds to the resulting amplitude used to bond the wires. Typical bonding strengths are in the area of 12 g while the tear strength of the wire is close to 16 g. The loss of strength is due to the fact that the wire is bent upwards after creating the bond, so it doesn't interfere with other components. The bending causes microscopic cracks to be formed in the bending area.

3.1.2.3 Jigs

To assemble the individual components, special single purpose jigs and tools were designed, reviewed, built and tested. Each jig is made with high accuracy, in order to be used during the production process. The main material of the jigs is aluminum. This makes them light and strong against twisting, bending and tearing. Yet, the silicon sensors can not touch the aluminum to avoid scratches on the sensor. These parts where the silicon sensors touch the jigs, are made from Delrin. Delrin was chosen because it is softer than silicon, which avoids scratches and glue does not adhere to its surface. This is important because the components are all glued together to form a ladder.

The purpose of these jigs is to hold, align or place the components within a matter of a few micrometers. The components are fixed to the jigs with vacuum. During assembly, a component is placed onto an alignment jig, where it can be aligned using special alignment tools. These tools are then removed and glue is applied

either per hand or with the CMM on the component. It is then placed on top of a second component, also aligned and fixed to a jig, to glue the two components together. The jigs are placed on top of each other using accurate linear bushings with an h5 accuracy of $+0mm$ and $-0.006mm$. The jigs stay in this position for 24h to make sure that the glue is completely cured. To build a complete ladder, a total of 28 different jigs were made, as seen on the next page.

3.1.2.4 Other devices

During the assembly, optical inspections have to be done in order to make sure that the ladder will work once it is finished. Microscopes are used to look at gluing patterns, wire bonds, bumps, cracks or other structures. Different inspections are done with different microscopes. During the Assembly, three microscopes will be used; the Nikon SMZ1000, the Olympus BX60 and the Leica Wild M3Z.

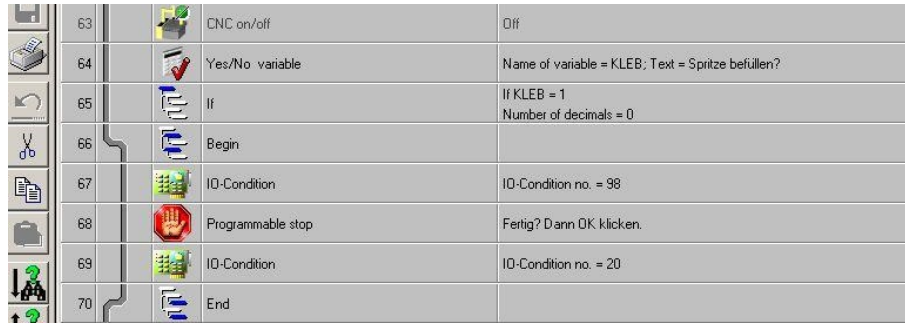
The sensor data is fed to microchips which are glued onto PCB boards next to the sensors. Hundreds of those chips are glued onto PCBs. The glue is applied with the CMM to the boards and an Essemtec Pantera XV Pick and Place robot will place the chips onto the boards. To apply the glue with the CMM, a gluing dispenser is used. This device can be programmed with the CMM software to apply air pressure to the needle where the glue is dispersed from. This method makes it possible to use the CMM as a gluing robot. The glue can be applied to the components while the CMM is driving and a signal to stop the air pressure will stop the glue from flowing.

3.1.3 Software

Software plays a vital role in assembling the ladders. The CMM, the gluing dispenser, the assembly stage and the electric tests require specialized software tools to function well. To configure and program the coordinate measuring machine, the original Mitutoyo software is used. The MCOSMOS (Mitutoyo Controlled Open Systems for Modular Operation Support) Geopak-Win Software uses a graphical user interface to control the machine and to develop measuring programs. These programs are based on single commands that are executed in a serial sequence (see figure 3.4). IF, WHILE, LOOP and GOTO commands can be used to further increase the extent of the program. The serial execution of commands, however is in case of the glue dispensing a negative point. The CMM will stop at the destined

3 Concept and SVD ladder design

coordinates, but it takes several milliseconds until the next command is executed, which stops the glue from flowing. This creates an irregular spread of the glue at the edges. To counteract to this effect, the machine will stop earlier, then turn the gluing dispenser off and then drive the rest of the path to help spread the glue more accurately. The completion of the different programs with all their functions was achieved in April 2015. Since then, the CMM software is continuously adjusted and developed further, to meet the high quality standards.



63	CNC on/off	Off
64	Yes/No variable	Name of variable = KLEB; Text = Spritze befüllen?
65	If	If KLEB = 1 Number of decimals = 0
66	Begin	
67	IO-Condition	IO-Condition no. = 98
68	Programmable stop	Fertig? Dann OK klicken.
69	IO-Condition	IO-Condition no. = 20
70	End	

Figure 3.4: Serial execution of steps

The CMM software developed for the assembly of a ladder includes:

- Gluing:
 - 'Glue flexible PCB's to sensors'
 - 'Glue Airex to sensors'
 - 'Glue flexible PCB CE onto Airex'
 - 'Glue flexible PCB -Z onto flexible PCB CE'
 - 'Glue flexible PCB's from underneath the sensor to flexible PCB's on thermal insulator'
 - 'Glue cooling clips onto flexible PCB CE and -Z'
 - 'Glue middle sensors to Rib'
- Measurement:
 - 'Rib measurement'
 - 'Alignment and measurement of sensor positions during production'

- 'Several different distance-, flatness-, angle- and diameter measurements'
- 'Sensor position measurement with analysis afterwards'

3.2 Ladder assembly procedure

3.2.1 Work flow chart

To produce a working detector module, each part needs to sit in the right place. The placement accuracy is controlled with the CMM. The CMM's accuracy is better, by at least a factor of ten, in comparison with the accuracy needed to build a ladder. The accuracy level of different parts are mostly defined by space constraints in the detector, but also, e.g. in case of the sensors, by the need for precision placement.

To consistently assemble ladders with equal accuracy, a work flow chart where every single step is documented, was developed. This ensures that the order of the steps and all the necessary know how is not mixed up or lost. Each step was considered carefully and tried out several times with different parameters before it was written down. The steps not only contain instructions on how to assemble a ladder, but also at which point, which test or measurement has to be done and how. The final layout and fine tuning of the procedure was made with focus on quality and practicality. The assembly procedure requires more than 100 steps to finish a ladder. Each step involves a series of tasks which have to be done step by step. To go through the complete procedure and finish a ladder takes between 12 and 15 workdays.

The procedure was first tested with dummy materials, such as an aluminum plate instead of a real silicon sensor. This way the real testing materials, which are rare and expensive, could be spared. After a rough draft of the procedure was set, it was first tested on a 'Class D' ladder. This ladder was made with real parts that are either not working or broken, although most of the procedure was proven to work that way. A 'Class C' ladder followed, where the assembly steps were refined. For the most part, adjustments concerned the accuracy of the alignment and the jigs. Next, a 'Class B' ladder was built which allowed further refinement of the procedure and the jigs. The work flow chart was adopted accordingly and after those three prototype ladders, it is ready for the production of 'Class A' ladders.

The work flow chart is divided into six parts:

- L5.1 Sensor + Flexible PCB Assembly
- L5.2 Rib Assembly
- L5.3 Flexible PCB Assembly Part 1
- L5.4 Ladder Assembly Part 1
- L5.5 Flexible PCB Assembly Part 2
- L5.6 Ladder Assembly Part 2

3.2.2 Assembly

Before each step, the required tools are prepared and cleaned with Isopropanol. Steps including the movement or touching of components require gloves. Before the assembly can start, several measurements are needed to assess the quality of the components. Each component is visually inspected and, if applicable, tested and measured; e.g. the Airex sheets need to have a certain thickness, and the electronic components on the PCB's need to be correctly connected and working. To measure the thickness of the sheets, the flatness of surfaces or the distances of e.g. drilling holes and alignment marks, the CMM is used. Measurement programs were made to automatically calculate and analyze the measured points, as well as writing this data, together with a diagram of the measured points into a PDF document for later use. Excel sheets (CSV) are also automatically created for further analysis.

3.2.2.1 L5.1 Sensor + flexible PCB assembly

As mentioned above, the ladder assembly is divided in six parts. In the first part, the two middle sensors are prepared for the ladder. One sensor is placed onto the sensor jig (see figure 3.5) and using an alignment tool, the sensor is aligned. The vacuum is turned on and holds the sensor in place. The alignment tool is then removed. Flexible PCB's ('pitch adapters') are aligned on their corresponding jigs (see figure 3.6 and 3.7) using alignment pins.

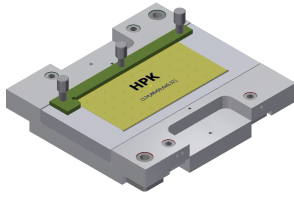


Figure 3.5: Sensor jig with alignment tool

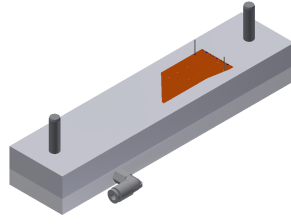


Figure 3.6: Flexible PCB jig 'PA1'

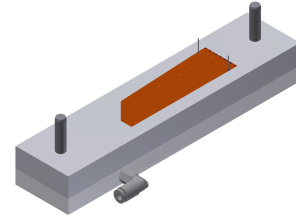


Figure 3.7: Flexible PCB jig 'PA2'

The CMM is used to automatically apply glue to the flexible PCB's. The program for this can be found under 'Gluing' and is called 'SPA'. A local coordinate system for each PCB is created by using alignment markers on it (see figure 3.8). The glue dispenser is set to 3.3 bars and the program must be followed as it contains all the necessary information to setup the CMM for gluing. After the glue is applied, the PCB jigs are turned around and placed on top of the sensor jig, using linear bushings (see figure 3.9). This will glue the flexible PCB's to the sensor. The vacuum is turned off now and after 24h the glue is cured. The PCB's can now be inspected under a microscope if the glue has spread under all the bonding pads (see figure 3.10).



Figure 3.8: Marker on PA1/2

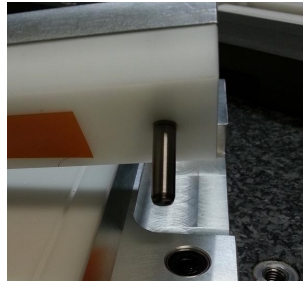


Figure 3.9: Glue flexible PCB to sensor

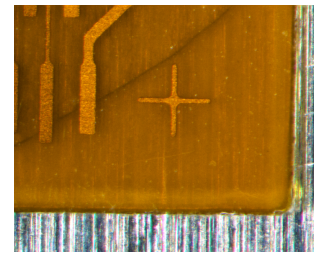


Figure 3.10: Optical inspection

The sensor is then again placed and aligned on the sensor jig. There, it will be electrically connected with the flexible PCB's, through wire bonding. The jig is placed on the wire bonding machine and the 'BELLE L5.1.70 spa' program is loaded. This program creates the inner wire bonds on the first PCB. After the wire bonds are applied, an optical inspection is done to see if the bonds are connected properly (see figure 3.11). Then, the programs for the inner wire bonds on the second PCB ('BELLE L5.1.71 spa'), the outer wire bonds for the first PCB ('BELLE L5.1.80 spa') and the outer wire bonds for the second PCB ('BELLE L5.1.81 spa') are executed one after the other with optical inspections in between.

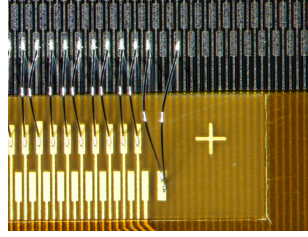


Figure 3.11: Wirebonds

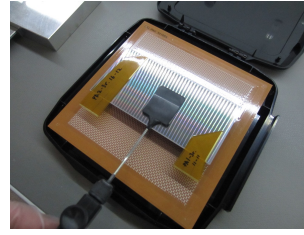


Figure 3.12: Storage box

The sensors are then stored in a box (see figure 3.12) where they are protected from external influences. The flexible PCB's on the sensors have a placement accuracy of up to $50\mu m$. This uncertainty is present because of the alignment and the placement of the jigs with the linear bushings. The accuracy of this gluing is sufficient because the bonding pads on the flexible PCB's do not have to be aligned more precise than roughly $500\mu m$ as the bonding machine can easily correct these displacements.

3.2.2.2 L5.2 Rib assembly

In the second part, the ribs are prepared. The forward endmount is assembled by installing the prism rail system (see figure 3.13), which is used as a sliding mechanism. This is done by inserting a ball, a spring and a screw in the two holes on the sides (see figure 3.14). Then the Kokeshi pin (see figure 3.15) is inserted in the prism (see figure 3.16). The prism is then slid into the forward endmount (see figure 3.17). Kapton tape is then glued onto the forward endmount (see figure 3.18) and a screw to fixate the Kokeshi pin is tightened with 40 Ncm. The forward endmount is placed onto the rib gluing jig (see figures 3.19 and 3.20). .

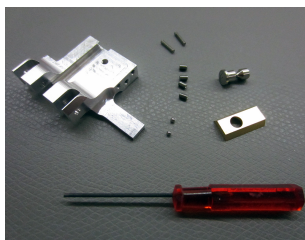


Figure 3.13: forward endmount

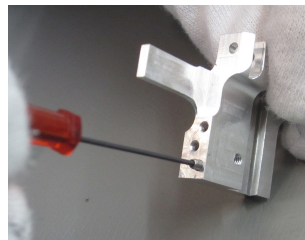


Figure 3.14: Installing prism rail

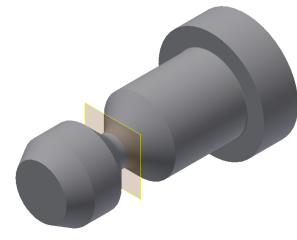


Figure 3.15: Kokeshi pin with indentation



Figure 3.16: Prism with Kokeshi pin

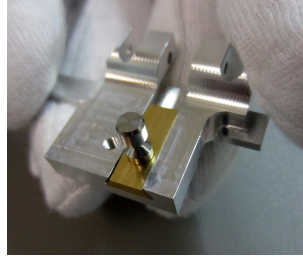


Figure 3.17: forward endmount finished

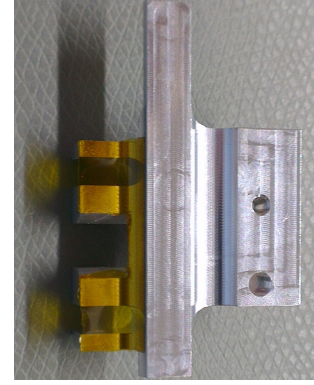


Figure 3.18: Kapton on forward endmount

The backward endmount is prepared by inserting a Kokeshi pin in it and placing it on the backward holder (see figure 3.21). Using the backward endmount alignment tool (see figure 3.22) it is aligned and fixated with a screw tightened with 40 Ncm. The two screws on top of the backward endmount are tightened as well. Then, Kapton tape is glued on the backward endmount (see figure 3.23). It is placed onto the rib gluing jig and a screw is inserted into the drilling hole on the top (see figure 3.24). The ribs are placed so they fit exactly into the gaps left out in the endmounts (see figure 3.25). The gaps are then filled with glue (see figure 3.26), so that the endmounts will be glued together with the ribs. Pins to fixate the endmounts and the ribs are inserted while the glue is still fresh (see figure 3.27).

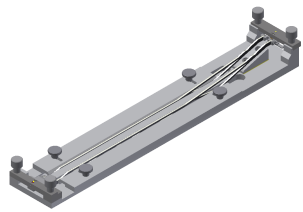


Figure 3.19: Rib gluing jig

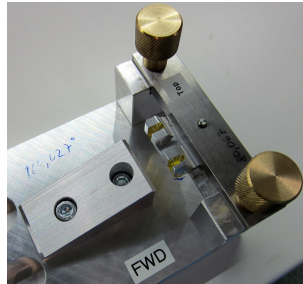


Figure 3.20: forward endmount placed

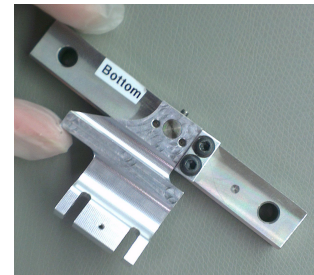


Figure 3.21: backward endmount on holder

3 Concept and SVD ladder design

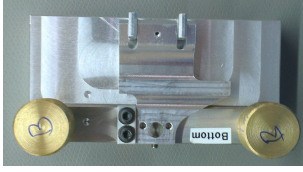


Figure 3.22: backward endmount alignment

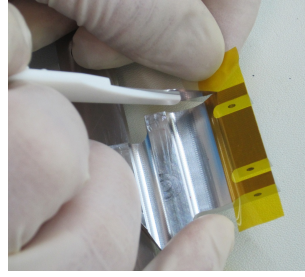


Figure 3.23: Kapton on backward endmount

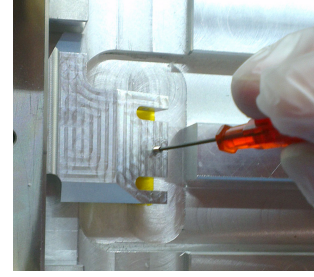


Figure 3.24: backward endmount placed

After 24h the glue is cured and the completed rib assembly is then mounted and fixed to the rib jig (see figure 3.28). A CMM measurement with a tactile measurement head that calculates the profile of the ribs follows (see figure 3.29). The ribs have protruding edges on which the sensors will be glued onto later (see figure 3.30). These edges are designed to form a flat surface. The real surface is calculated from fifteen measurement points on each edge. The CMM measurement is completely automated once the position of the ribs on the CMM surface is known. The information of this measurement is used to check the accuracy of the ribs. Large offsets are a reason to dismiss a rib assembly.

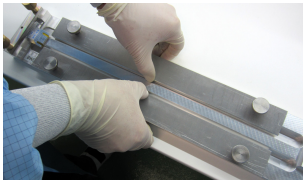


Figure 3.25: Placing ribs into endmounts

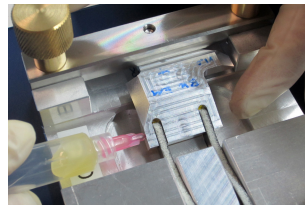


Figure 3.26: Glue endmounts to ribs

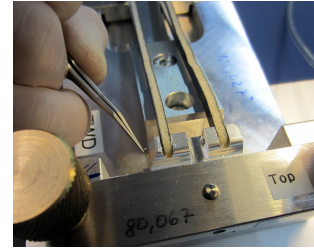


Figure 3.27: Insert pins on both sides

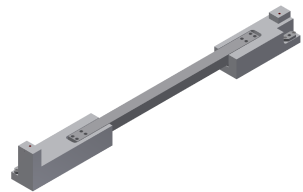


Figure 3.28: Rib jig to mount rib assembly

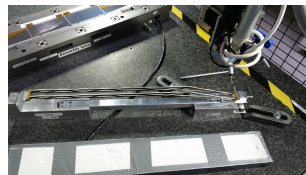


Figure 3.29: CMM measurement

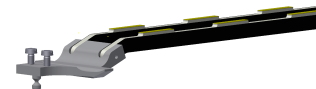


Figure 3.30: Protruding edges on ribs

3.2.2.3 L5.3 Flexible PCB assembly part 1

The third part addresses the sensor alignment. The forward and backward sensor inlay jigs (see figures 3.31 and 3.32) and the assembly bench (see figure 3.33) are placed on top of the assembly base (see figure 3.34) using linear bushings. The assembly bench is fixed on the CMM surface to avoid accidental movements.

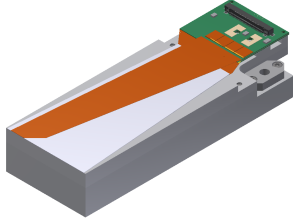


Figure 3.31: forward sensor inlay with sensor

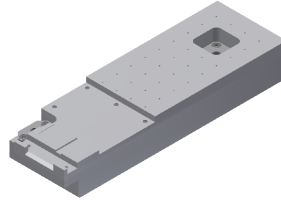


Figure 3.32: backward sensor inlay

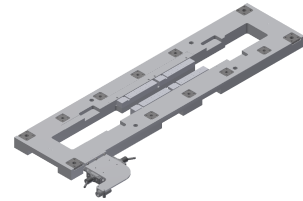


Figure 3.33: Assembly bench



Figure 3.34: forward and backward sensor inlays and assembly bench on assembly base

The forward sensor (see figure 3.35) is picked up from its transport jig with the forward pick up jig using linear bushings to guide the jig and vacuum to transfer the sensor. The forward pick up jig is then placed on the assembly bench using linear bushings (see figure 3.36). Once the vacuum is switched off on the forward pick up jig and on on the assembly bench, the forward pick up jig can be removed. The same procedure is done with the backward sensor (see figure 3.37) on the backward transport jig.

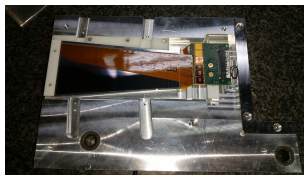


Figure 3.35: forward sensor on transport jig

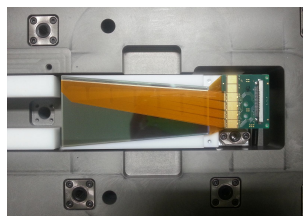


Figure 3.36: forward sensor on assembly bench

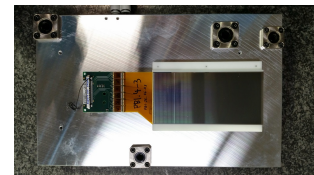


Figure 3.37: backward sensor on pick up jig

3 Concept and SVD ladder design

The two sensors are then slid outwards from the middle of the bench by roughly $100\mu m$ using the XYZ theta alignment stage. The two middle sensors with the flexible PCB's and wire bonds already attached (see figure 3.38) are aligned one after the other on the sensor jig and then placed on the assembly bench (see figure 3.39) using linear bushings. Using the XYZ theta alignment stages and the CMM, the four sensors are aligned on the assembly bench (see figure 3.40). The XYZ theta alignment stages are placed on top of the sensors and grab them with vacuum. Micrometer screws can be used to adjust the position of a sensor in X and Y direction, as well as the angle through rotation of the sensor.

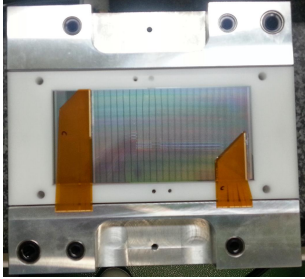


Figure 3.38: Middle sensor on sensor jig

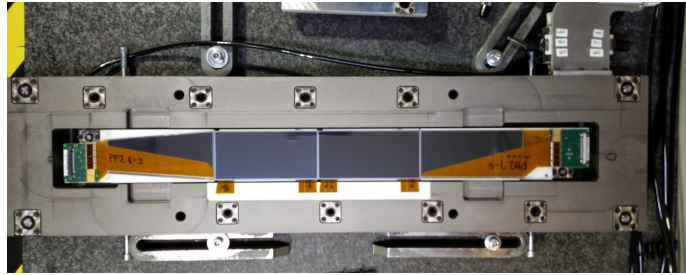


Figure 3.39: All sensors placed on assembly bench after alignment

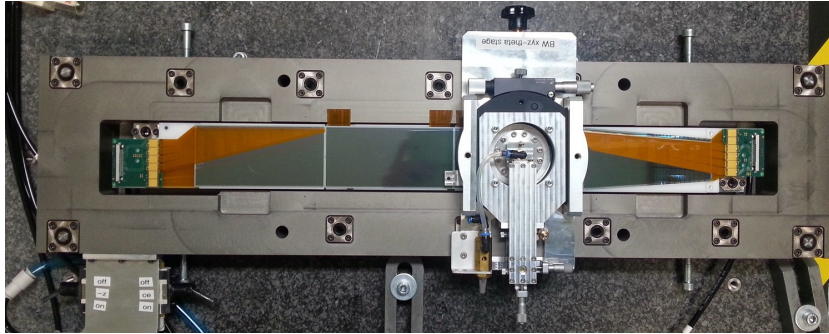


Figure 3.40: Using the XYZ theta alignment stage to align the sensors

The design distance between two sensors is $120\mu m$. The uncertainty of the micrometer screws of the stages with the platform the sensor is held on to is in the area of $\pm 5\mu m$. The uncertainty of the optical CMM system accounts for further $\pm 10\mu m$. The largest uncertainty comes from the XYZ theta alignment stage. The sensor is held above the resting surface of the assembly bench by vacuum. The distance is set manually with a screw between 20 and $200\mu m$. The lower the distance, the lower the uncertainty of the placement due to the sensor dropping down to the assembly bench. But, as the thickness of the silicon sensors can vary by up to $50\mu m$, the sensor must be lifted upwards to move it. If the sensor touches the

resting surface on the assembly bench during movement it could take scratches or even break.

The average uncertainty of the drop from the vacuum holder to the assembly bench is $\pm 30\mu m$ with a maximum measured uncertainty of $\pm 50\mu m$. This happens because the air underneath the sensor forms an air cushion when the sensor is lowered by gravity. This causes the sensor to move. Added up, the sensor placement is still possible within the design range. To lower the uncertainty and maximize the accuracy of the sensor positions, the vacuum holder from the XYZ theta alignment stage is lowered until it touches the sensor slightly. The vacuum is switched on and then the sensor is lifted upwards. After aligning the same process in reverse is done to avoid the forming of an air cushion on which the sensor lands. Then the vacuum on the assembly bench is switched on again and the XYZ theta alignment stage is taken off. The offset from this procedure is lowered by almost a factor of ten.

After the XYZ theta alignment stage is placed on the assembly bench the 'Align Sensors' program on the CMM can be loaded. Once the position of the assembly bench is known, the CMM drives to the design position and using the XYZ theta alignment stages, the sensors are aligned. After all four sensors are aligned and lowered back to the assembly bench, the CMM automatically drives to the design position on each edge of each sensor. In this case, alignment markers (see figure 3.41) on the silicon sensors are used. Then the machine will be manually driven to the exact point of the alignment marker. After all sixteen measurement points are done, the CMM calculates the offsets of all sensors and the distances between them.

In the last step the forward and backward sensors are removed with the backward jig (see figure 3.42) and the forward jig (see figure 3.43). Linear bushings are used to guide the jigs into position (see figure 3.44) and PCB clamps (see figure 3.45) are used to fix the PCB's to the jigs. These two jigs are designed to keep the alignment of the sensors during storage (see figure 3.46) and the eventual gluing to the ribs.

3 Concept and SVD ladder design



Figure 3.41: Alignment marker on sensor

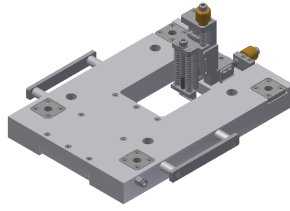


Figure 3.42: Backward jig with PCB clamp

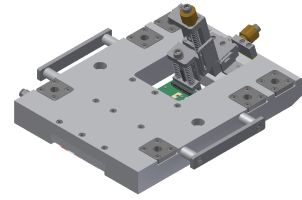


Figure 3.43: Forward jig with PCB clamp

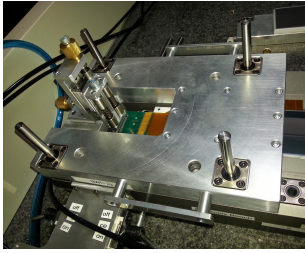


Figure 3.44: backward jig on assembly bench

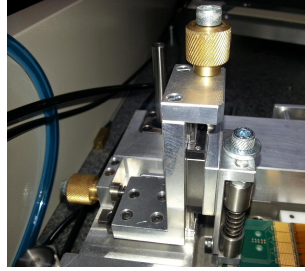


Figure 3.45: Micrometer screw for PCB clamp

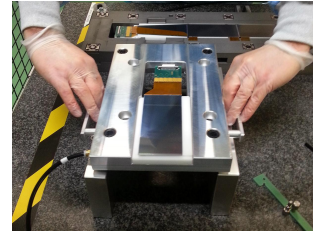


Figure 3.46: backward sensor on backward jig

3.2.2.4 L5.4 Ladder assembly part 1

Part four describes the gluing of the outer two sensors on the rib assembly. The rib jig with the mounted ribs as well as forward and backward spacers are placed on top of the assembly base using linear bushings (see figure 3.47). Before the sensors are glued to the ribs, thermal conductive tape is applied onto the forward and backward endmounts (see figures 3.48 and 3.49). The PCB clamp on the forward jig is manually driven into the position marked on the clamp (see figure 3.50).

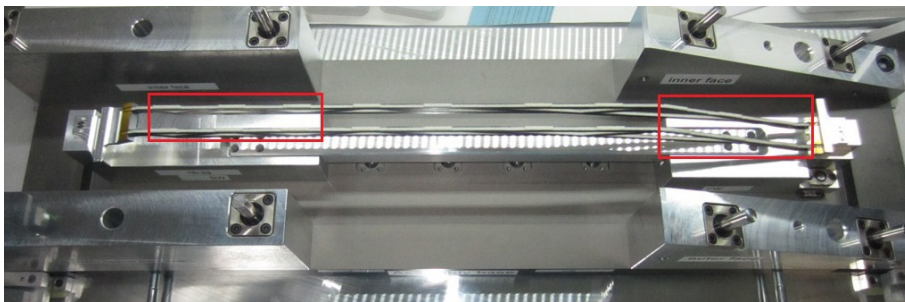


Figure 3.47: Rib jig, forward and backward spacers on assembly base

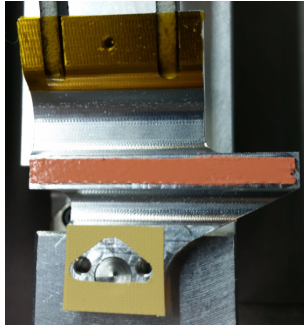


Figure 3.48: backward endmount with thermal tape

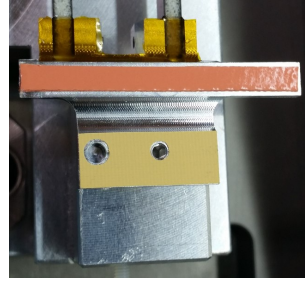


Figure 3.49: forward endmount with thermal tape

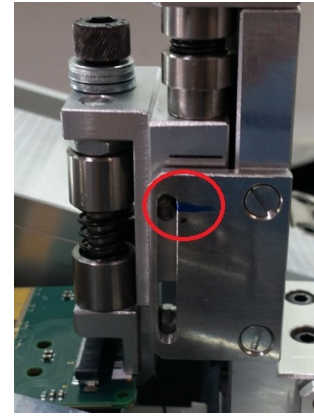


Figure 3.50: PCB clamp with micrometer screw on forward jig

Glue is manually applied to the protruding edges of the ribs. The forward and backward jig with the sensors still fixed to them, are then placed on top of the forward and backward spacers (see figures 3.51 and 3.52). Once on, the sensors will directly be glued onto the ribs. After 24h the glue is cured, the forward and backward jigs and the forward and backward spacers are removed and the forward and backward sensors will already be in their final resting position (see figure 3.53).

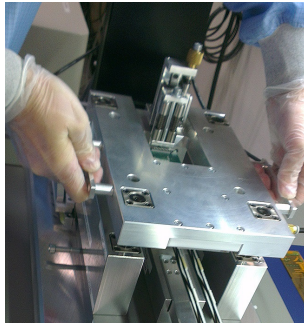


Figure 3.51: backward jig lowered to rib using spacers

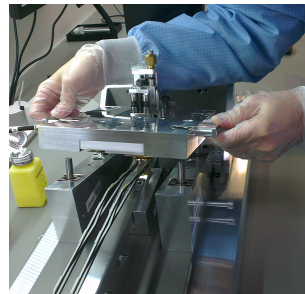


Figure 3.52: forward jig lowered to rib using spacers



Figure 3.53: backward and forward sensors glued to rib

The forward and backward APV guards that protect the APV's from damage during handling are prepared by applying thermal conductive tape on it (see figures 3.54 and 3.55). The forward and backward APV guards are then placed on top of the PCB's with a vacuum pen and the screws on both APV guards are tightened (see figure 3.56). This connects the APV guards with the PCB's and the endmounts underneath. A spacer that separates the PCB's on the forward and

3 Concept and SVD ladder design

backward sides from the PCB's that will be attached in later steps on top of it, is glued onto the PCB (see figure 3.57).

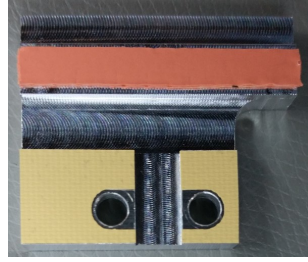


Figure 3.54: backward APV guard with thermal tape

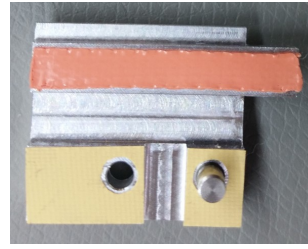


Figure 3.55: forward APV guard with thermal tape

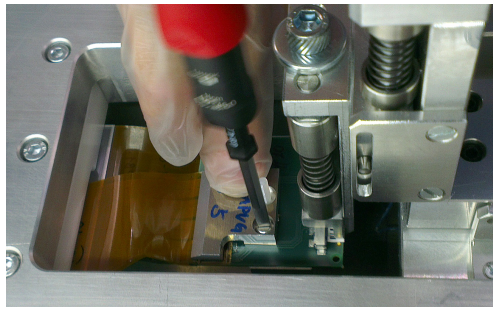


Figure 3.56: backward APV guard screwed to rib

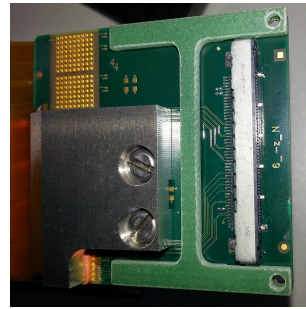


Figure 3.57: PCB separator glued to PCB

The rib assembly is designed to be completely flat on top of the protruding edges. Due to manufacturing uncertainties, bending of the ribs and thermodynamic influences, the rib assembly is not flat. The height of the protruding edges increases continuously towards the bent part of the ribs. An error of up to $150\mu m$ can be measured. The design height is reached only at the very first and last protruding edge on each rib. The ladder design, however intends to place the sensors on a flat surface in a defined height. The difference in height of the top of the protruding edges and the bottom part of the sensors is compensated by the glue that holds the parts together. The amount of glue is identical on every protruding edge. Towards the outer edges, the glue will be squeezed out less, than on the middle ones. The design distance between the protruding edges and the sensors is $200\mu m$.

3.2.2.5 L5.5 Flexible PCB assembly part 2

In part five the flexible PCB's that connect the sensors to the electronics are glued on. The assembly is prepared by removing the backward sensor inlay jig

and replacing it with the backward dummy jig (see figure 3.58). This jig has a larger cut out so that the flexible PCB's can be placed. A dummy sensor is placed onto the backward dummy jig (see figure 3.59) which acts as a spacer. A sheet of thermal insulator material ('Airex') is cut out using a cutting tool and a knife (see figure 3.60). The sheet has to be large enough to cover the bonding pads of the flexible PCB's above it. The minimum size of it is defined by the cutting tool. The maximum size is defined by the bonding pads on the sensor. The sheet cannot cover any of them in order for the ladder to work. The difference between the minimum and maximum size of the sheet is roughly 2mm. It is then aligned using a special alignment tool (see figure 3.61) on the thermal insulator jig (see figure 3.62).

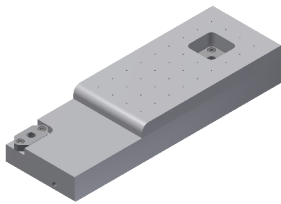


Figure 3.58: backward inlay dummy jig with extra cut out for PCB's



Figure 3.59: backward dummy sensor on backward inlay dummy jig



Figure 3.60: Cut out Thermal insulator sheet 'Airex'

The 'Airex' program on the CMM is used for the sheet. To apply the glue, the position of the alignment tool is used as a reference. After the position is known by the CMM the alignment tool is removed and the glue is applied. Using linear bushings the thermal insulator jig is placed onto the assembly bench (see figure 3.63). The thermal insulator is now glued on top of the two middle sensors that are still aligned on the assembly bench.



Figure 3.61: Thermal insulator sheet alignment tool

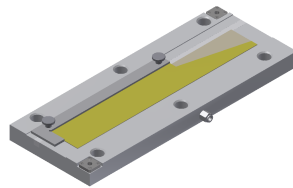


Figure 3.62: Thermal insulator sheet jig with alignment tool



Figure 3.63: Gluing thermal insulator to sensors

After 24h the long flexible PCB ('Origami CE') can be glued on top of the thermal insulator. The long flexible PCB is placed on its alignment jig (see figure 3.64) and

3 Concept and SVD ladder design

using two pins, it is aligned. It is important that the PCB's are aligned well, so that the bonding process can work. Otherwise the bonding pads can be inaccessible. The long flexible PCB is then transferred from the alignment jig to its gluing jig (see figure 3.65) with linear bushings.

The 'Origami CE' program on the CMM is used to manually drive to four defined positions on the PCB sheet (see figure 3.66). These positions are used as a reference for the CMM. The glue is then applied by the CMM automatically. Using linear bushings the gluing jig with the long flexible PCB is placed on the assembly bench. After 24h the glue is cured and the gluing jig is removed (see figure 3.67). The short flexible PCB ('Origami -Z') is aligned with the short flexible PCB alignment jig and glued with the short flexible PCB gluing jig in the same way the long flexible PCB was glued (see figure 3.68).

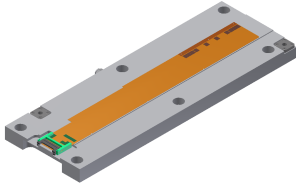


Figure 3.64: Long flexible PCB 'Origami CE' alignment jig

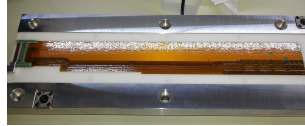


Figure 3.65: Long flexible PCB 'Origami CE' gluing jig

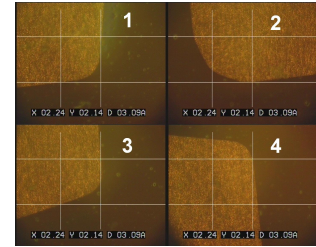


Figure 3.66: Alignment positions on flexible 'Origami' PCB's

After the glue is cured the assembly bench is placed on the wire bonding machine. The 'BELLE L5.5.90 sensor n pa0' program is loaded and wire bonds which connect the upper side of the sensors with both flexible PCB's are created. To test the strength of these wire bonds, some test wire bonds are pulled off and the necessary force is measured (see figure 3.69). Then the 'BELLE L5.5.100 pa0 apv n inner row' program is loaded for a second row of wire bonds between the sensors and the flexible PCB's. The assembly bench is now placed in a black box and connected to the APV DAQ system. An electrical test is performed to check if the wire bonds are all working. Defective wire bonds are repaired manually. As soon as all the wire bonds are working the assembly bench is placed on the wire bonding machine again. The 'BELLE L5.5.110 pa0 apv n outer row' program is used to apply further wire bonds.

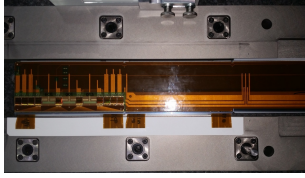


Figure 3.67: Long flexible PCB 'Origami CE' glued

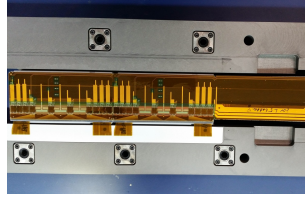


Figure 3.68: Short flexible PCB 'Origami -Z' glued

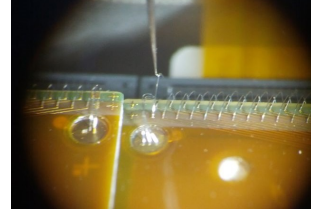


Figure 3.69: Wire bonds pulled off to measure strength

To connect the lower side of the sensors, the short flexible PCB's (from part L5.1) glued onto the lower side of the sensors have to be bent around for 180°, using the bending jig (see figure 3.70). They and will then be glued to the larger flexible PCB's already glued onto the top of the thermal insulator. The glue is applied with the CMM (see figure 3.71) using the 'PA bending' program. A push down jig is used to push the flexible PCB's down to the assembly bench (see figure 3.71). After the glue is applied the assembly bench is placed under a microscope on the assembly table (see figure 3.72). The microscope is used to watch the bending procedure in detail.

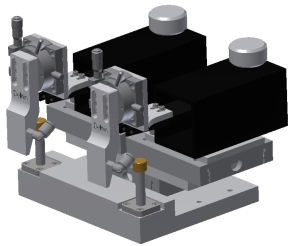


Figure 3.70: Bending jig with micro positioners and vacuum nozzles

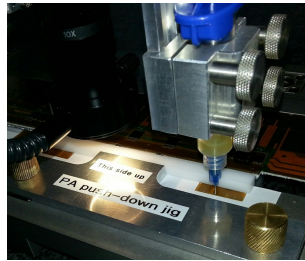


Figure 3.71: Applying glue on the flexible 'pitch adapter' PCB's

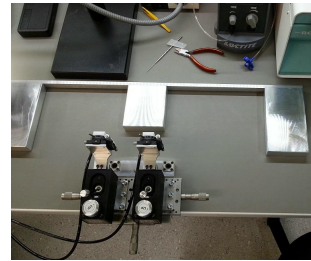


Figure 3.72: Assembly table and bending jig under microscope

The flexible PCB's are bent with the pre bend jig (see figure 3.73) and the bending jig is placed and fixed to the assembly bench with linear bushings. The bending jig uses two micro positioners with a vacuum nozzle in the front which holds the flexible PCB's. The positioners can be moved by micrometer screws with an uncertainty of $\pm 5\mu m$. The flexible PCB's are placed with the glue on them onto the top of the assembly (see figure 3.74). The distance between the PCB's and the surface determines how well the glue spreads out. For the subsequent wire bonding to work, the area under all the bonding pads has to be covered. Once the distance is short enough that the glue touches the surface the microscope can be used to view the gluing process.

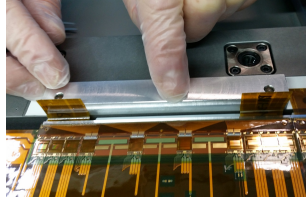


Figure 3.73: bending flexible PCB's with pre bend jig

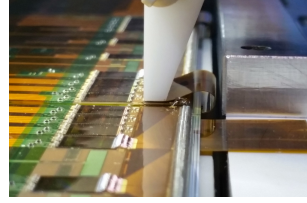


Figure 3.74: Gluing flexible PCB to surface with bending jig

After all four flexible PCB's are bent around and glued, they will be wire bonded to the APV chips. The 'BELLE L5.5.140 pa12 apv p inner row' program on the wire bonding machine is used for that. Further wire bonds for the bias voltage are created with the 'BELLE L5.5.152 pa2 bias' and the 'BELLE L5.5.152 pa1 bias' programs. An electrical test using the APV DAQ system checks if all new wire bonds are working. After the electrical test further wire bonds are created using the 'BELLE L5.5.160 pa12 apv p middle row' and the 'BELLE L5.5.160 pa12 apv p outer row' programs on the wire bonding machine. A last electrical test with the APV DAQ system checks those wire bonds.

3.2.2.6 L5.6 Ladder assembly part 2

Part six describes the assembly to finish the ladder. The assembly stage with the two drivable paddles is placed on top of the CMM surface (see figure 3.75). It is controlled by a LabView program which allows to calibrate and move the stages synchronously upwards and downwards with an accuracy of a few micrometers. The assembly base with the rib jig, which holds the ladder sub assembly created in L5.4, is placed on top of the assembly stage (see figure 3.76). The CMM is used to apply glue onto the ribs and the backward sensor with the 'Ribs and sensor' program. The position of the rib jig is used as a reference for the gluing lines. Once this is known, the CMM automatically applies glue on the protruding edges of the ribs (see figure 3.77) and on the backward sensor (see figure 3.78).

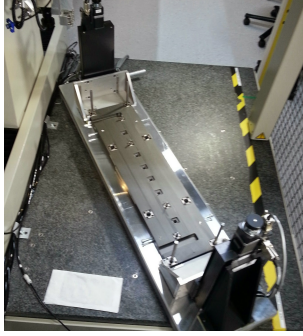


Figure 3.75: Assembly stage and assembly base on CMM surface



Figure 3.76: Rib assembly on assembly base on CMM surface



Figure 3.77: Applying glue on the protruding edges

When it is applied, the two paddles of the assembly stage will sync their movement and drive upwards, above the ladder sub assembly (see figure 3.79), using a LabView program. The assembly bench with the middle sensors on it will be placed on the paddles above the ribs and using the LabView program the paddles are lowered to the exact height of the the ribs (see figure 3.80). The uncertainty of this placement is less than $\pm 5\mu m$. The lateral placement is defined by the prior sensor alignment, as the sensors are still in the same position as they were after the alignment. When the paddles reach their position, the middle sensors will touch the glue on the protruding edges of the rib and the overhanging flexible PCB will be glued to the backward sensor. The glue is cured after 24h.

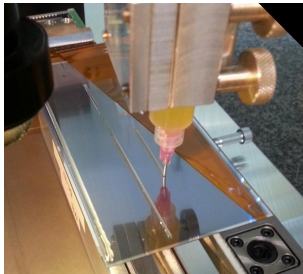


Figure 3.78: Applying glue on the backward sensor with CMM

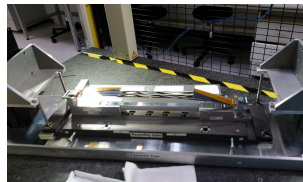


Figure 3.79: Assembly stage with paddles driven up



Figure 3.80: Assembly bench lowered to rib assembly

Cooling clips are then attached to the top of the assembly using the cooling clip jig (see figure 3.81). The clips are attached to the jig and glue is applied on them manually (see figure 3.82). The cooling clip jig is placed on the assembly bench which is still lying on the paddles of the assembly stage, using linear bushings (see figure 3.83). The placement of the cooling clips has an uncertainty of $\pm 50\mu m$.

3 Concept and SVD ladder design

which is acceptable as the cooling clips are several millimeters away from critical components. After 24h the cooling clip jig is removed and the clips will stick to the ladder assembly (see figure 3.84).



Figure 3.81: Cooling clip jig



Figure 3.82: Glue applied to cooling clips

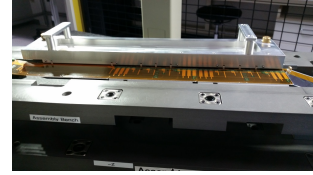


Figure 3.83: Cooling clip jig on assembly bench

By turning off the vacuum on the assembly bench the middle sensors will be detached from it and using the paddles of the assembly stage the assembly bench can be lowered down onto the assembly base (see figure 3.85). The ladder which is screwed onto the rib jig can now be removed. The PCB boards on the forward and backward sides of the ladder are glued and screwed together (see figure 3.86). After the glue is cured, the ladder is finished (see figure 3.87). The CMM is used to measure the sensor positions and the geometry of the ladder with the 'Ladder measurement' program (see 3.2.3).

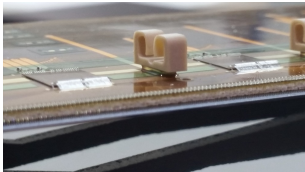


Figure 3.84: Cooling clip glued to ladder



Figure 3.85: Assembly bench lowered down

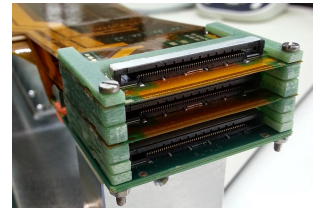


Figure 3.86: PCB's screwed together

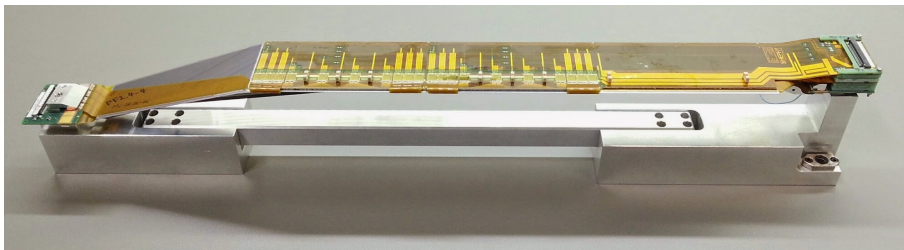


Figure 3.87: Finished ladder on rib jig

Summarizing, the most critical placement procedure is the positioning of all of the flexible PCB's. If the distance between the surface and the PCB is too large the glue will not spread and will not cover the area under the bond pads. If it is too

short the glue will be pushed out underneath the PCB's and cover wire bonding pads on the outside. If the PCB's are glued on slightly rotated the overhanging part can either block wire bonds or reach over the edge of the gluing surface and not be glued at all. In these cases wire bonding will not be possible.

3.2.3 After production

After the assembly is finished, the sensor positions are measured, this time in their final resting position on the ribs after the glue has cured. This is the position that the sensors will be in, when they are built into the Belle II detector. The positioning information of this measurement is used as a starting point for the alignment algorithms applied for each physics run.

The measurement of the ladders is performed with the CMM. A measurement program was made which is able to take measurements and create a statistical analysis. The calculations are done in the program on the fly which not only saves time, but also minimizes the factor of the human error of these calculations. The software creates a special coordinate system on the rib jig, that is equal for every single L5 ladder built. The coordinate system was aligned using the two drilling holes on top of the rib jig. The software creates a center point at each drilling holes in the height of the backward hole. Connecting a line from the backward hole to the forward hole gives the positive X axis. Turning the line 90° to the left around the backward hole gives the positive Y axis. Turning the line another 90° from both axes in an upward direction gives the positive Z axis. The zero point is in the center of the backward hole. A visualization of the coordinate system can be seen in figure 3.88.

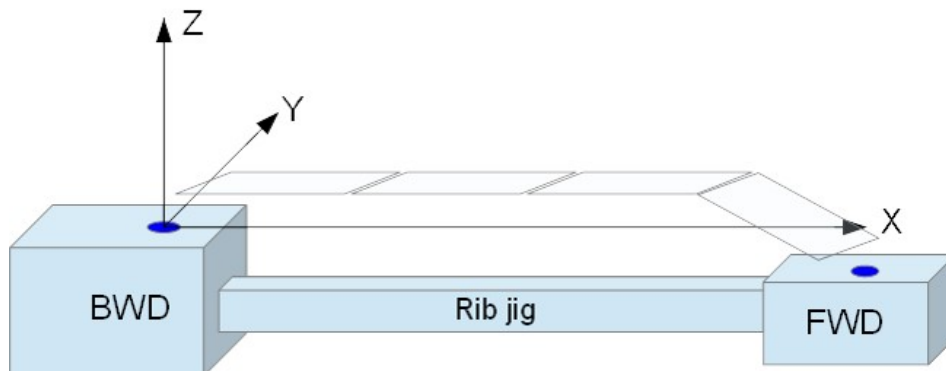


Figure 3.88: Alignment of the coordinate system on the Rib jig

3 Concept and SVD ladder design

Each corner of the four sensors has a name; h, f, e and g (see figure 3.89). In every corner is a F marker for alignment which is approached by using the optical sensor of the CMM. For each sensor, a set of four X, Y and Z coordinates is taken. The result is a set of 16 coordinates. The coordinates are firstly compared to the nominal coordinates and the offset of each set of sensor coordinates is calculated. In the next step, the distances between the sensors is calculated. This is done with two separate measurements. Once the distance between the F positions is calculated from the initial measured values. This is the F - F distance which can be seen in table 4.5 for the class D ladder. It has an exact nominal value and can be compared and interpreted easily. The coordinate system on a sensor can be seen in figure 3.90.

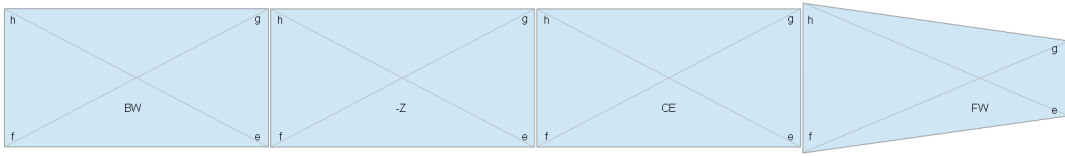


Figure 3.89: Sensors orientated as on a ladder with corner names h, f, e and g

In a second step, the actual cutting edges of the sensors are measured, with which the gap between the sensors is calculated. This measurement is important because of the sensors cutting edge uncertainty of $\pm 40\mu m$ given by the manufacturer of the sensors. This measurement therefore determines whether two adjacent sensors are touching each other or not. The nominal distance between two sensors is $900\mu m$. If two sensors are in physical contact with each other, this could result in shorts, scratches or cracks on the sensors. Even if the sensors are not quite touching each other by a few micrometers, the assembly needs to be interrupted and reevaluated, because the ribs on which they are glued on, can expand and contract over time, depending on the temperature, which could put mechanical stress on the sensors.

After the offsets and distances are calculated, the angles α , β and γ (see figure 3.91) of each sensor are calculated. The results of all calculations are stored in a .csv file. This ladder measurement is done four times to minimize random errors and enabling statistical analysis. The systematic errors in this case, are the positioning errors in X, Y and Z of the CMM and the placement errors of the jigs. The latter can be minimized by building prototypes and adjusting the assembly procedure.

With the information of the corners points of each sensor, several calculations can

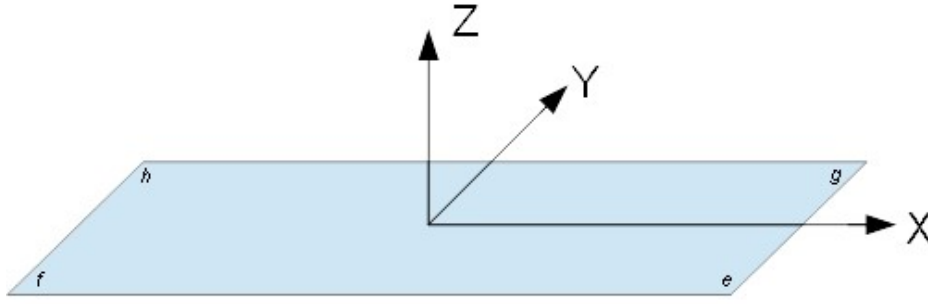


Figure 3.90: Coordinate system on the sensor with corner names h, f, e and g

be made:

- the offset of each point compared to the nominal values in X, Y and Z direction
- the overall offset of each sensor in X, Y and Z direction
- the distances between the sensors including their offsets
- the angle of each sensor around the X, Y and Z axis

On the finished ladder, the sensors are placed almost completely flat, but small angles can still be measured. Because the nominal side lengths of the sensor are known and the coordinates of the sensors are measured, all three lengths in the theoretical rectangular trigonometric triangle are known. Using the tangent and the sine functions, the angles can be calculated (see figure 3.91).

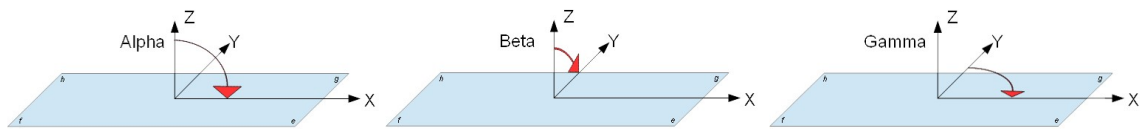


Figure 3.91: Alpha, Beta and Gamma angles on the sensors

Alpha, which is the angle rotating around the Y axis, is calculated using the height differences of the sensor on the two longer sides. Alpha is positive when looking from the positive Y axis to the origin, the X and Z axis rotate clockwise. Since there are four measured points, the calculation is done twice, once for the left side and once for the right side. The height difference is $\Delta Z_{ef} = \text{height}_e - \text{height}_f$ for one side and $\Delta Z_{gh} = \text{height}_g - \text{height}_h$ for the other side. Alpha is then

3 Concept and SVD ladder design

calculated by using the sine function:

$$\alpha = \frac{\arcsin\left(\frac{\Delta Z_{ef}}{\text{Nominal_sensor_length}}\right) + \arcsin\left(\frac{\Delta Z_{gh}}{\text{Nominal_sensor_length}}\right)}{2}$$

Beta is the angle rotating around the X axis. Beta is positive when looking from the positive X axis to the origin, the Z and Y axis rotate clockwise. It is calculated in the same manner as Alpha, yet this time the offset in the Z direction from the shorter sides of the sensors are used. $\Delta Z_{hf} = \text{height}_h - \text{height}_f$ for one side and $\Delta Z_{ge} = \text{height}_g - \text{height}_e$ for the other side. Beta is then calculated by again using the sine function:

$$\beta = \frac{\arcsin\left(\frac{\Delta Z_{hf}}{\text{Nominal_sensor_width}}\right) + \arcsin\left(\frac{\Delta Z_{ge}}{\text{Nominal_sensor_width}}\right)}{2}$$

Gamma is the angle rotating around the Z axis. Gamma is positive when looking from the positive Z axis to the origin, the X and Y axis rotate clockwise. The longer sides of the sensors are used to calculate the angle using the offsets in Y direction. The Y offset is $\Delta Y_{gh} = \text{width}_g - \text{width}_h$ for one side and $\Delta Y_{ef} = \text{width}_e - \text{width}_f$ for the other side. Gamma is then calculated by using the sine function:

$$\gamma = \frac{\arcsin\left(\frac{\Delta Y_{gh}}{\text{Nominal_sensor_length}}\right) + \arcsin\left(\frac{\Delta Y_{ef}}{\text{Nominal_sensor_length}}\right)}{2}$$

The Alpha and Beta angles occur because of mechanical inaccuracies of the jigs. Changes in the procedure or in the sensor alignment wouldn't make any differences. Gamma is the only angle that can be minimized with precise sensor alignment. The better the sensor alignment is, the closer are the F marker on the sensors to their nominal positions. Less offset in X and Y direction minimizes the Gamma angle.

The precision for a class A ladder is not defined as such, but by working closely together with the other institutes, that build ladders for the Belle II detector, some accuracy levels can be defined. To directly compare the measurement results of the different institutes, the room temperature of the assembly clean room is measured as well. The ladder measurements take place at the same room temperature of 24°C.

The same measurement is also done with the prototypes after artificial aging using thermo cycles in a climate chamber, where the temperature is varied 60 times between -5°C up to 70°C . The results of this measurement after the thermo cycling can be seen for the class B ladder in figure 3.92. It shows slightly more accurate values for the X coordinate and less accurate values for the Y direction. The Z direction shows better values for the backward and -Z sensor and worse values for the CE and forward sensor. The changes are of little significance as they are very low. This means that the aging process of the ladders will not be problematic when the ladders are working in the detector. As mentioned earlier, the sensor position on the ladder is a quality criteria, yet this time, after the completion of the ladder, the sensors can't be moved and aligned again.

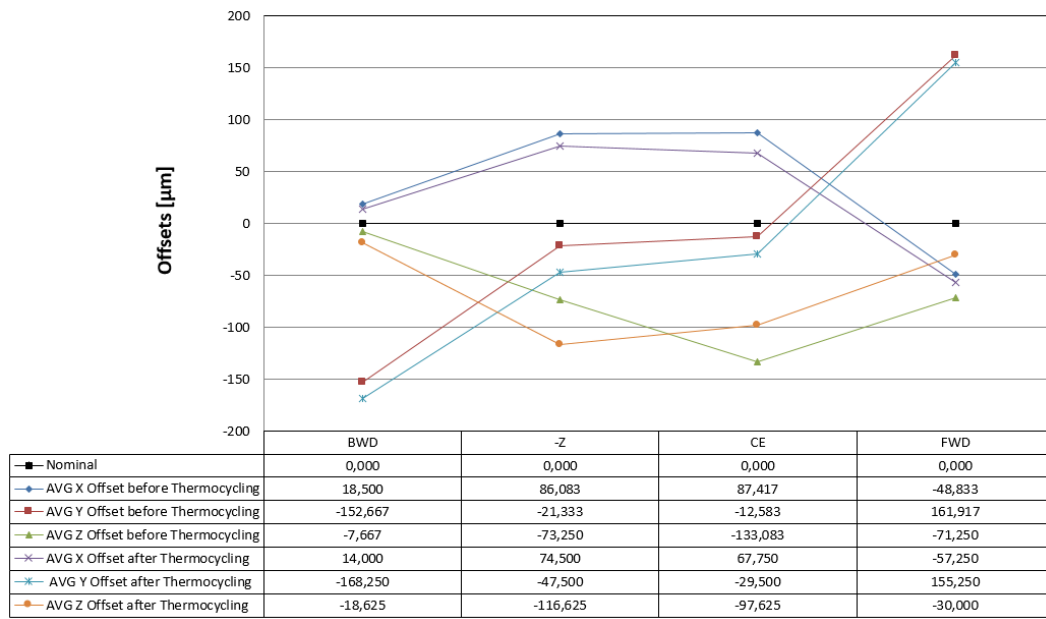


Figure 3.92: X, Y and Z offsets to the nominal value before and after thermo cycling on the class B ladder

4 SVD ladder assembly

4.1 Building the first prototype

4.1.1 Assembly

The assembly procedure was tested each part for its own. These procedures were improved up to the point where they were thought to suit the ladder assembly well. The challenge of this separated procedures was to think about eventual issues or interferences while using the procedure during the assembly of a complete ladder, where all the other components are added as well. Building a first prototype was therefore necessary to validate and improve the assembly procedure. Each step was carefully executed and documented.

Major adjustments of the assembly procedure were not needed, yet countless smaller improvements were implemented. The changes were tested on dummies, made only for the purpose of testing these changes. The dummies don't consist of original components and are not created according to the assembly procedure. They were simplified to save time building them and to only fulfill their purpose.

The forward and backward sensor transport jig as well as the cooling clip jig were not ready to be used during this production. The prototype was therefore not built exactly according to the assembly protocol. The left out steps could not be verified. The accuracy of the first prototype however, was not influenced by this. The forward and backward sensors were placed by hand instead of the jig and later aligned with the XYZ theta alignment stages. The cooling clips were not attached. Errors and operational mistakes during the assembly included the loss of vacuum after the sensor alignment, the shifting of sensors after the thermal insulator sheet was already glued and the pulling at a PCB because of a misfitting jig. The sensor alignment of the middle sensors was done by hand as the thermal

insulator sheet prevented the usage of the XYZ theta alignment stages. The sensor alignment therefore was lost and couldn't be recovered. The ladder was finished though, to test all following steps.

The expected accuracy of the sensor alignment after the vacuum was lost, was less than $200\mu m$. The values of the other components were expected to be close to the accuracy values needed for class A ladders. Due to the fact that assembly jigs were missing and the vacuum was lost, the ladder didn't classify as a class C ladder. It was therefore renamed a class D ladder. Overall, the ladder was finished in the given time frame and most of the assembly steps could be proven to work.

4.1.2 Measurements and evaluation

The finished Class D ladder was measured with the CMM. A separate measurement program was not ready to measure the ladder automatically. The manual measurement did not introduce any further measuring inaccuracies, as the coordinate system alignment is equal, compared to a separate program. The program would allow for much faster and more comfortable measurements. This is the reason why such a measurement program was created later. Table 4.1 shows the sensor alignment with the XYZ theta alignment stage at the beginning of the assembly. Only the X and Y offsets are measured, since the sensors are lying flat on the assembly bench in their default Z position.

It can be seen that the -Z sensor is not as well aligned as the other sensors. During this early state of the production, the alignment procedure could not be consistently performed and the measurement was not as accurate as it will be later on further prototypes. One reason for the additional offset of the -Z sensor is that during taking off the XYZ theta alignment stage, the sensor shifted in the X direction.

The measurements were taken after the XYZ theta alignment stage was already removed from the sensors, therefore the measurement includes a possible additional shift during removal of it. The sensors were fixed by vacuum to the assembly bench in their aligned positions. The numbers suggest a very good alignment of the sensors. Although after looking more closely into the procedure, it was discovered that the sensors were not lifted up by the XYZ theta alignment stage, but the stage was actually pressing the sensor down slightly, thereby dragging the sensor

Sensor	Position	X offset [μm]	Y offset [μm]
BWD	h	1	-3
	f	1	-3
	e	-3	-12
	g	2	-17
-Z	h	-57	-44
	f	-50	-65
	e	-48	-48
	g	-59	-29
CE	h	0	-26
	f	8	-12
	e	-3	-64
	g	1	-40
FWD	h	-5	-35
	f	-3	-15
	e	-1	15
	g	1	-53

Table 4.1: Offsets of all sensors after alignment for class D ladder. h, f, e and g denote the sensor edges (see figure 3.90)

across the surface of the assembly bench. This caused irreversible scratches on the sensors. The procedure would have meant for the XYZ theta alignment stage to lift up the sensor, holding it by vacuum, then aligning it in X and Y direction, and then disconnecting the vacuum to let the sensor glide down onto the assembly bench, where it is held in place by the vacuum of the assembly bench.

Since the sensors thickness varies between 280 and 320 μm , the XYZ theta alignment stage cannot hold the sensor just a few micro meters above the surface in order to not scratch the sensor while moving it. The actual distance that the sensor is lifted upwards is up to 200 μm . The sensor is aligned in this height to make sure dust or other particles cannot affect the integrity of the sensor. However, this creates an air cushion below the sensor, on which it lands while gliding down. This causes the sensor to move in a random direction, creating an additional offset, which is measured on all subsequent ladders.

Turning on the vacuum of the assembly bench first, before turning off the vacuum which holds the sensor on the XYZ theta alignment stage, causes the sensor to be pulled downwards onto the assembly bench. This almost removes the effect of the air cushion, but since the sensor is only held with vacuum on one side, because of

the mechanical design, this causes the sensor to being pulled downwards unevenly, which again creates a random offset. This method however, is less controllable than letting the sensor glide down on an air cushion, therefore this method was quickly abandoned again. During the class D sensor alignment, this air cushion was not formed, therefore this offset was never introduced. The sensors however are left with scratches which could have a negative effect on the performance. Since the class D ladder is not electrically working, the effects of the scratches can never be tested. The sensors on the following ladders will be handled differently during alignment. The XYZ theta alignment stage is used to pick up the sensors at a very close range with vacuum. Then, once the sensor is held by the stage, it is moved farther upwards and aligned. After alignment, the XYZ theta alignment stage is used to drive down the sensors close to the surface and the vacuum is switched. This way, the effect of random offsets is minimized. A first test showed offsets of close to $5\mu m$.

The three tables below (4.2, 4.3 and 4.4) show an analysis of the measured offsets on the finished ladder, separated for each sensor. Each table represents another coordinate system direction. The offsets are given for each sensor position (h, f, e, g) and an averaged value for each sensor is calculated. The measurement was done four times, to make sure that the measurement error of the CMM and of the optical system are not distorting the actual sensor positions. There is also a small positioning uncertainty when placing the ladder onto the rib jig which could also take part in distorting the sensor positions. Four measurements allow for calculating the arithmetic mean values, the measured extreme values, the median and the standard deviation. On this ladder, the positioning uncertainty was measurable, yet compared to the sensor offsets, the influence of the errors was small.

Sensor	Position	X [μm]				
		Arith. Mean x	Min x	Max x	Median x	Std. dev.
BWD	h	54	48	66	51	8
	f	-5	-11	6	-8	8
	e	N/A	N/A	N/A	N/A	N/A
	g	-7	-14	5	-10	9
	AVG	14	8	26	11	8
-Z	h	111	106	124	107	9
	f	71	65	82	69	8
	e	109	104	119	106	7
	g	73	67	84	70	8
	AVG	91	86	102	88	8
CE	h	N/A	N/A	N/A	N/A	N/A
	f	81	76	92	79	8
	e	115	109	126	112	8
	g	80	73	91	78	8
	AVG	92	86	103	89	8
FWD	h	-68	-75	-57	-70	8
	f	-151	-160	-139	-152	9
	e	-64	-71	-52	-67	8
	g	-38	-44	-26	-40	8
	AVG	-80	-88	-69	-82	9

Table 4.2: X offsets of the sensors on finished class D ladder

Sensor	Position	Y [μm]				
		Arith. Mean y	Min y	Max y	Median y	Std. dev.
BWD	h	-58	-60	-55	-58	2
	f	-59	-62	-57	-59	2
	e	N/A	N/A	N/A	N/A	N/A
	g	72	68	74	73	3
	AVG	15	-18	-13	-15	2
-Z	h	-30	-32	-29	-30	1
	f	-30	-32	-28	-30	2
	e	50	46	51	51	2
	g	48	45	49	49	2
	AVG	9	7	11	10	2
CE	h	N/A	N/A	N/A	N/A	N/A
	f	65	63	67	66	2
	e	139	137	141	139	2
	g	138	136	140	139	2
	AVG	114	112	116	114	2
FWD	h	-114	-116	-113	-114	1
	f	-109	-112	-106	-109	2
	e	17	15	21	16	3
	g	19	18	21	19	2
	AVG	-47	-49	-44	-47	2

Table 4.3: Y offsets of the sensors on finished class D ladder

Sensor	Position	Z [μm]				
		Arith. Mean z	Min z	Max z	Median z	Std. dev.
BWD	h	-120	-125	-108	-124	8
	f	-312	-316	-305	-313	5
	e	N/A	N/A	N/A	N/A	N/A
	g	-242	-250	-227	-245	10
	AVG	-224	-230	-213	-227	8
-Z	h	-107	-120	-95	-107	10
	f	-210	-226	-196	-209	14
	e	-140	-149	-133	-139	7
	g	-251	-264	-236	-251	12
	AVG	-177	-190	-165	-176	11
CE	h	N/A	N/A	N/A	N/A	N/A
	f	-282	-287	-274	-284	6
	e	-133	-153	-114	-133	16
	g	-242	-269	-209	-246	27
	AVG	-219	-236	-199	-221	16
FWD	h	-18	-39	-4	-14	17
	f	-98	-134	-80	-89	25
	e	-36	-54	-26	-31	13
	g	228	211	237	231	12
	AVG	19	-4	32	24	17

Table 4.4: Z offsets of the sensors on finished class D ladder

It can be seen that the backward sensor and the CE sensor are each missing one measurement point. In both cases, the marker on the sensor was covered by the flexible PCB sheets on top of the sensors. These sheets have a cut out on the marker positions, but the positioning was bad due to a mechanical error of the gluing jig. This error caused the flexible PCB sheet to be misaligned on the jig, even before it was placed. Those sensor coordinates could not be measured and were left out of the calculation process of the offsets. Since these sensors have still three other measured points, the error of this missing values is minor.

The average offsets of the Z coordinates are much larger than the offsets in X and Y direction. The backward sensor and the two middle sensors are more than $200\mu m$ lower than they should be. The only time when the Z coordinate of the middle sensors is defined, is during the descent with the assembly stage. The backward sensor is also lower than expected, yet this sensor was placed with the backward jig, which has a defined height, very close to the nominal value. The measured values suggest that the descending sensors are placed correctly, but that the ladder itself is lifted upwards by $200\mu m$. After some mechanical fine tuning of the erroneous pins that caused the rib jig to be lifted upwards, the Z height was corrected. The Class B ladder was built with this correction in place and shows a smaller Z offset (see figure 4.7).

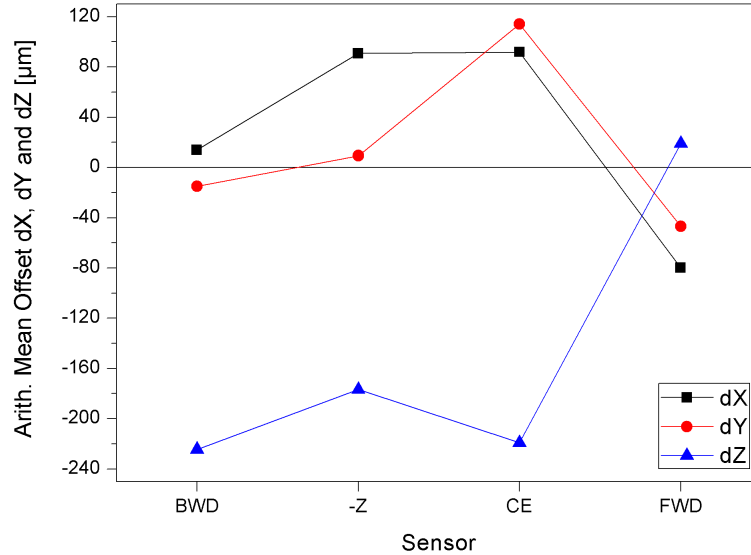


Figure 4.1: Average offset to the nominal values per sensor on class D ladder

Figure 4.1 shows the offset per sensor averaged over the four measurement points on one sensor and over the four separate measurements taken. It clearly shows the large Z offset caused by the rib jig. A shift in the X direction of the -Z and CE sensor shows that a more precise alignment has to be done.

The CE sensor is too far shifted in the positive Y direction ($114\mu m$). The distance between the sensors are nominal $120 \pm 40\mu m$. The measured sensor distances, averaged over the four measurements, can be found in table 4.5. The sensor distances are measured by their nominal offset of the nominal F positions and by their actual cutting edge distances. The sensors are not overlapping and they are not touching each other. The reason for this is, that all the rectangular sensors are shifted in a positive Y direction. While the forward sensor is shifted in the -Y direction, its 16° angle, and a small cutting edge helps to provide a gap between the CE and the forward sensor.

Sensor	F - F distance [mm] Nominal 0.9 mm	actual cutting edge distance [mm] Nominal $120 \pm 40\mu m$
BWD - -Z	1.018	0.177
-Z - CE	0.968	0.070
CE - FWD	0.927	0.223

Table 4.5: Averaged sensor distances on the class D ladder

The distance of the cutting edges deviates from the nominal $120 \pm 40\mu m$. These values correlate with the measured Y offsets of the sensors. The large offsets will be reduced in the following prototypes, due to the better alignment of the sensors and the improved procedures.

With the offset values from tables 4.2, 4.3 and 4.4, the angles of all sensors can be calculated as seen in 3.2.3. Table 4.6 shows the averaged angles around the X, Y and Z axes for each sensor.

Sensor	$d\alpha$ AVG [$^\circ$]	$d\beta$ AVG [$^\circ$]	$d\gamma$ AVG [$^\circ$]
BWD	-0.028	0.060	-0.128
-Z	-0.017	0.104	-0.037
CE	0.036	0.069	-0.034
FWD	-15.927	-0.147	-0.059

Table 4.6: Averaged offset of the sensor angles to the nominal values on the class D ladder

It can be seen that alpha on the forward sensor is 15.927° . This angle is off by 0.073° . All the other angles nominally should be zero. The angle β on the

forward sensor is noticeably larger than on the other sensors. The sensor was placed according to the procedure set, yet the quality of the ribs themselves may have been compromised, as well as the fact that the measurement procedure was done without a measurement program which would have reduced the measurement errors.

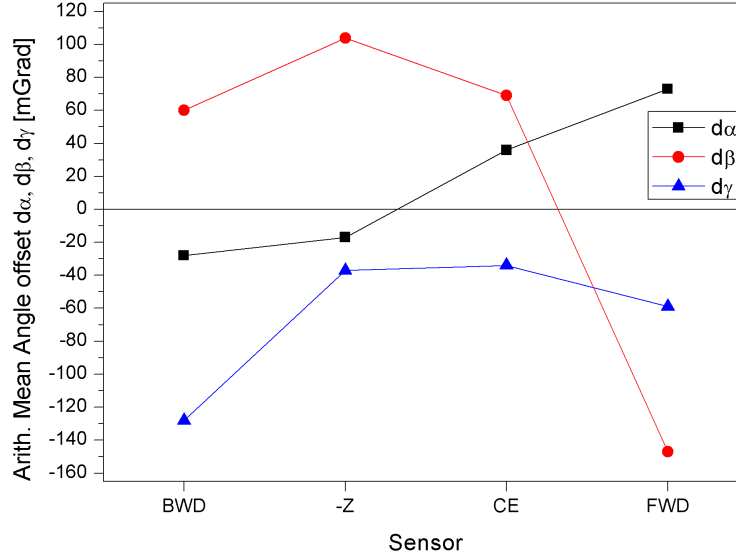


Figure 4.2: Averaged offset of the sensor angles to the nominal values on the class D ladder

As there are no clear tolerance levels defined, the angles are hard to interpret, because even little angles can cause a large offset on one point. The table shows angle offsets of more than $|0.1^\circ|$ which, at one side can lead to an offset of $218\mu m$ as seen in figure 4.3. The side length of the triangle is the sensor length of 124.1mm. Therefore, angles as low as possible are needed for the assembly.

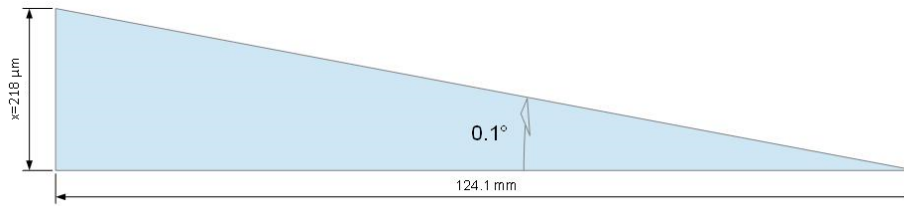


Figure 4.3: Max offset with an angle of 0.1°

The accuracy level measured on this ladder was as expected. There was still some mechanical fine tuning necessary to achieve a more precise ladder.

4.2 Further progress

4.2.1 Class C prototype

The class D ladder was mainly built to test the procedures and the jigs which were used for the assembly. The accuracy was not expected to be perfect from the start. Some mechanical changes were made during and after the assembly to reach a better accuracy and to fix design issues. Programs for the ladder measurement, with automatic calculation of offsets and angles were developed and the assembly procedure was revised.

After reproducing the measurement errors of the class D ladder and correcting them, the production of a class C ladder with mechanically final components was attempted. The assembly was done exactly according to the procedure which means, that an increase in accuracy was expected. The ladder was built with class C sensors and chips, which means that they are either not tested or known to not work as they should. The ladder can still be electronically tested, but the results are of no importance on this ladder.

The assembly itself worked without any problems. The revision of the procedures and the jigs was thereby validated. Table 4.7 shows the sensor alignment on the class C ladder. The Y offsets of the -Z and the CE sensor are still large, but in general, compared to the class D ladder, the improvement of the alignment procedure worked well.

Sensor	Avg. X offset [μm]	Avg. Y offset [μm]
BWD	-8	4
-Z	7	38
CE	-1	46
FWD	2	5

Table 4.7: Offsets of all sensors to the nominal values on class C ladder after alignment

The ladder was finished within twelve working days. Table 4.8 shows the sensor positions on the finished class C ladder. As on the class D ladder before, the same Z offset appeared, making it clear that there is a systematical error involved. Afterwards, the rib jig was adjusted, and early measurements suggest, that the error was removed. It will be shown later in table 4.12 that the error disappeared for the class B ladder.

Sensor	Avg. X [μm]	Avg. Y [μm]	Avg. Z [μm]
BWD	65	63	-213
-Z	129	122	-221
CE	140	97	-208
FWD	-122	171	-149

Table 4.8: Averaged sensor offsets to the nominal values on finished class C ladder

Figure 4.4 displays the negative Z values as well as correlating sensor offsets for the backward and the two middle sensors. It also shows that the forward sensor has very different offsets. A large shift in Y direction of more than $70\mu m$ compared to the already shifted CE sensor can be observed. The forward sensor is also shifted in -X direction, with still leaving a gap between the CE and forward sensors as seen in 4.9.

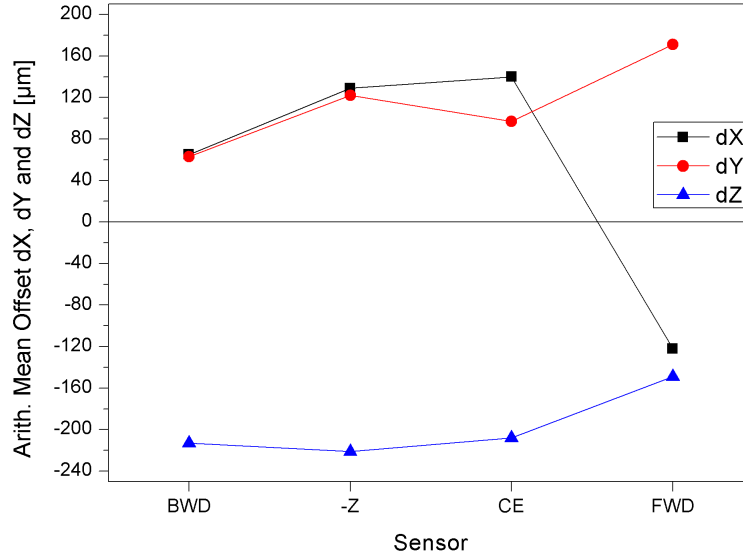


Figure 4.4: Averaged sensor offsets to the nominal values on finished class C ladder

Large offsets can be seen in all coordinate directions. The source of the offset of the Z coordinates have already been identified as an error of the rib jig. The X and Y offsets of the -Z, CE and forward sensors are too large. Correcting these offsets can be done by adjusting the position of the assembly bench on the assembly stage during the final descent. This will not be done before the next ladder assembly as proof of these offsets is still needed in form of a consistent offset values with the following class B ladder.

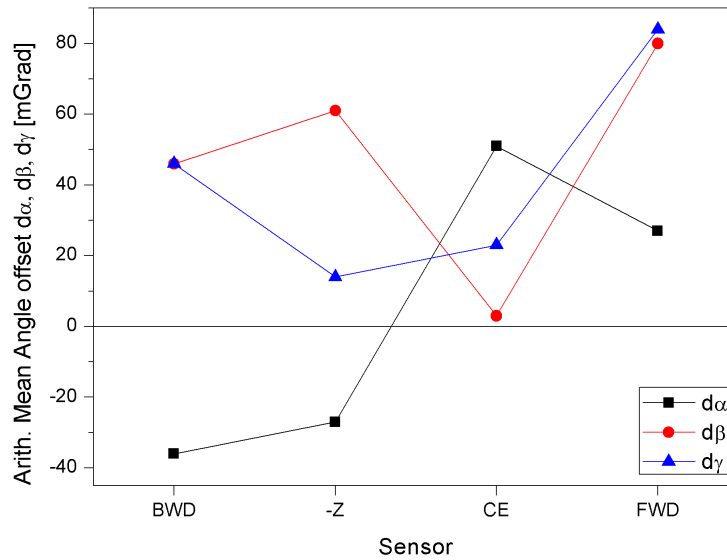
Sensor	F - F distance [mm]	actual cutting edge distance [mm]
BWD - -Z	0.991	0.162
-Z - CE	0.930	0.089
CE - FWD	0.855	0.192

Table 4.9: Averaged sensor distances on finished class C ladder

It can be seen in table 4.9 that the distances between the sensors are good. The distance between the two sensors on the backward side is larger than expected, and the one between the sensors on the forward side is lower than expected. These smaller and larger distances are corresponding to the sensor offsets seen in 4.4.

Table 4.10 and figure 4.5 show the averaged offset of the angles from the nominal angle. The offsets are lower, compared to the class D ladder, by almost a factor of 2. The offset values are good and could, except for the forward sensor, which can still be improved, be accepted on a class A ladder as well.

As seen in figure 4.10, the alpha angles on all sensors are acceptable on all sensors. Beta on the forward sensor might be adjusted with the forward jig, while gamma will be more accurate as soon as the source for the X and Y offsets are corrected. This will happen after the next ladder is built.

**Figure 4.5:** Average angle per sensor on finished class C ladder

Sensor	Alpha AVG [°]	Beta AVG [°]	Gamma AVG [°]
BWD	-0.036	0.046	0.046
-Z	-0.027	0.061	0.014
CE	0.051	0.003	0.023
FWD	-15.973	0.080	0.084

Table 4.10: Averaged sensor angles on finished class C ladder

4.2.2 Class B prototype

After again revising the procedures and adjusting the jigs, a new prototype could be built. To electronically test a ladder and interpret its data signals, a class B ladder was assembled in this step. This ladder requires working sensors and wire bonds. The need for precise positioning of the components on this ladder is important, as it can only be read out correctly if all the wire bonds are in their place and working well. Misaligned components could damage or brake the wire bonds easily.

The temperature during this assembly was on average 23.9°C . The following table 4.11 shows the detailed offsets of the sensor alignment with the XYZ theta alignment stage at the beginning of the assembly. The alignment procedure was repeated until the alignment offset on each sensor was minimal. The backward sensor was least well aligned, but with very low offsets still.

Sensor	Avg. X offset [μm]	Avg. Y offset [μm]
BWD	27	-21
-Z	-5	-1
CE	2	2
FWD	9	2

Table 4.11: Offsets of all sensors after alignment on class B ladder

After the alignment, the ladder was finished. At a first glance the ladder looked very promising, but during the electrical testing it was shown that each sensor had segments, where the signals showed errors. It was discovered that the sensor jig, which was used to place the -Z and CE sensors on the assembly bench, was not cut out correctly. Wirebonds on the forward and backward sensors on every prototype were damaged until this discovery (see figure 4.6). Since the earlier ladders were not electrically tested, this error never showed itself before. A revision of the sensor jig, with a larger cut out removed the error.

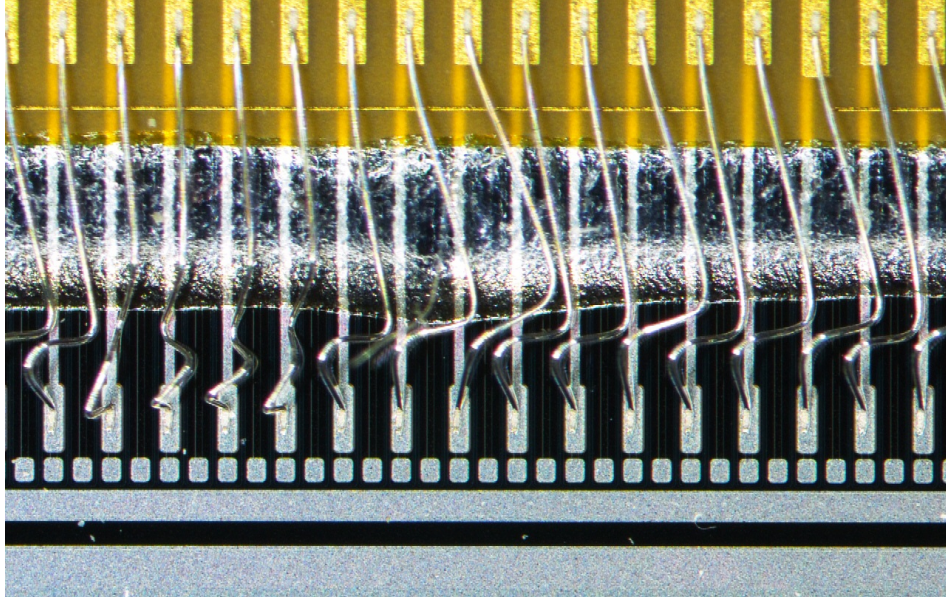


Figure 4.6: Damaged and bent wire bonds between the sensor and a flexible PCB on class B ladder. Glue spread out under flexible PCB is normal.

The average offsets of the sensors on the finished class B ladder can be seen in table 4.12. Figure 4.7 visualizes the result. The offset in X direction is good on the forward and backward sensors, but rather large on the -Z and CE sensors. The opposite can be said for the offsets in Y direction. They are very good on the -Z and CE, but bad on the forward and backward sensors.

Sensor	Avg. X [μm]	Avg. Y [μm]	Avg. Z [μm]
BWD	17	-158	-16
-Z	84	-28	-87
CE	84	-18	-137
FWD	-51	159	-69

Table 4.12: Averaged sensor offsets of class B ladder

The rib jig was revised and the Z offsets are better now. The Z offset is very good on the backward sensor, larger on the -Z sensor and even more larger on the CE sensor. This trend is also seen when the ribs are measured during the rib assembly. Mechanical tension that compresses the ribs slightly causes this bending. One possible solution is to glue the ribs further into the forward and backward endmounts, to counteract to the compression. This solution will be tested during the next prototype assembly.

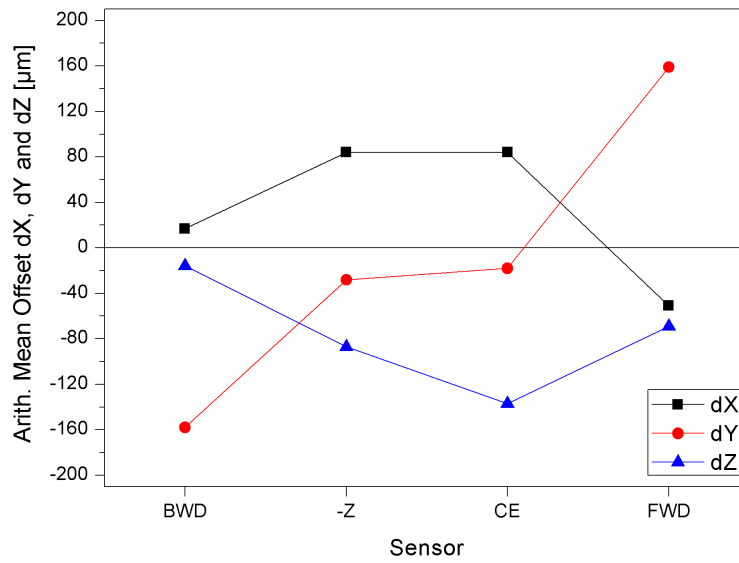


Figure 4.7: Average offset per sensor on class B ladder

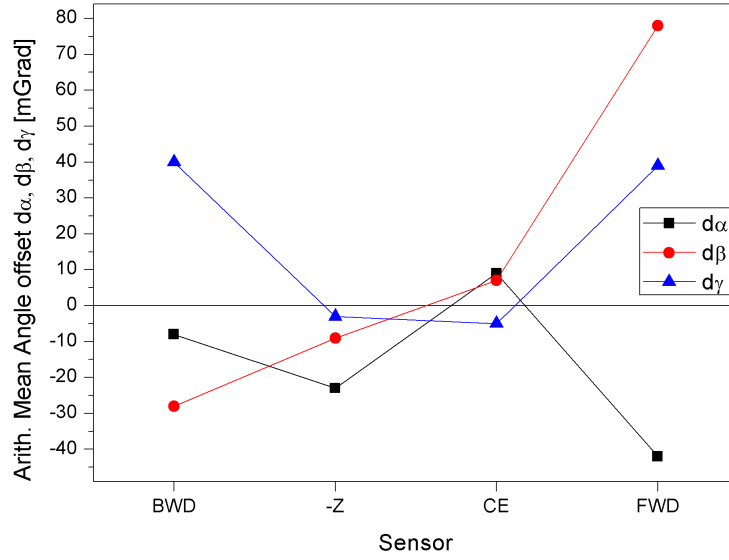
Table 4.13 shows the distances between the sensors. The results show that the distances between two sensors on the backward side and also between the two sensors on the forward side is too large. This can also be seen with the Y offsets in table 4.12. The distances would be good, if the forward and backward offset would be smaller.

Sensor	F - F distance [mm]	actual cutting edge distance [mm]
BWD - -Z	0.951	0.232
-Z - CE	0.903	0.166
CE - FWD	0.975	0.361

Table 4.13: Averaged sensor distances on class B ladder

Table 4.14 shows the measured offsets of the angles on the finished class B ladder on every sensor. The angles on the -Z and CE sensor are very small and qualify for a class A assembly. The angle offsets on the backward sensor are larger, but still good. The forward sensor shows larger offsets of all three angles as can be seen in 4.8. The gamma rotation is small enough, but alpha and beta are too large. A study will be made to gain information on how to avoid or correct this shifts.

Sensor	Alpha AVG [°]	Beta AVG [°]	Gamma AVG [°]
BWD	-0.008	-0.028	0.040
-Z	-0.023	-0.009	-0.003
CE	0.009	0.007	-0.005
FWD	-16.042	0.078	0.039

Table 4.14: Averaged sensor angles on class B ladder**Figure 4.8:** Average angle per sensor on class B ladder

4.2.3 Summary and Results

A total of three L5 ladder prototypes were built.

- A first class D prototype to test the procedures
- A class C prototype to refine and tweak the procedures
- A class B prototype with working sensors, to be able to perform electrical tests

The production of these ladders showed where improvement in mechanical accuracy is necessary and where corrections and adjustments had to be done. The overall offsets of the sensors averaged over the whole ladders has been reduced significantly during the assembly. This can be seen in figure 4.9.

In comparison, it can be seen that the class D ladder had very low X and Y offsets. The reason for this is, that the sensors were dragged over the surface during alignment, scratching them in the process. This was resolved for the class C and class B ladders. Larger offsets in X and Y were the consequence. The class B ladder however, was built with improved jigs and procedures and a drop in offsets in X and Y direction can be seen.

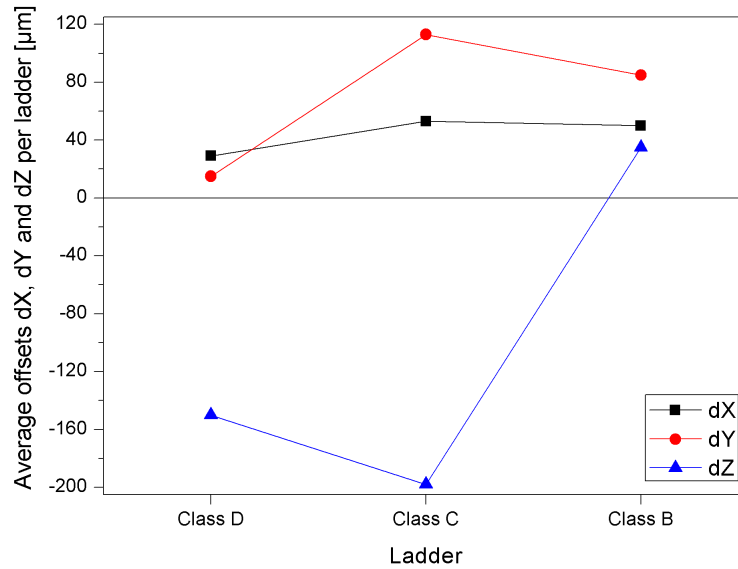


Figure 4.9: Average offset per ladder on class B ladder

The Z offset was caused by a drilling hole on the rib jig which was too short. As soon as the hole was deepened (after the assembly of the class C ladder), the average Z height is close to the nominal value. The same trend can be observed for the angles of the sensors. Figure 4.10 shows a very large gamma offset on the class D ladder which was caused by rough alignment and unfinished procedures. After some tweaking, the class C ladder showed a much smaller gamma angle. With refined procedures, the following class B ladder showed even lower offsets of the gamma angle.

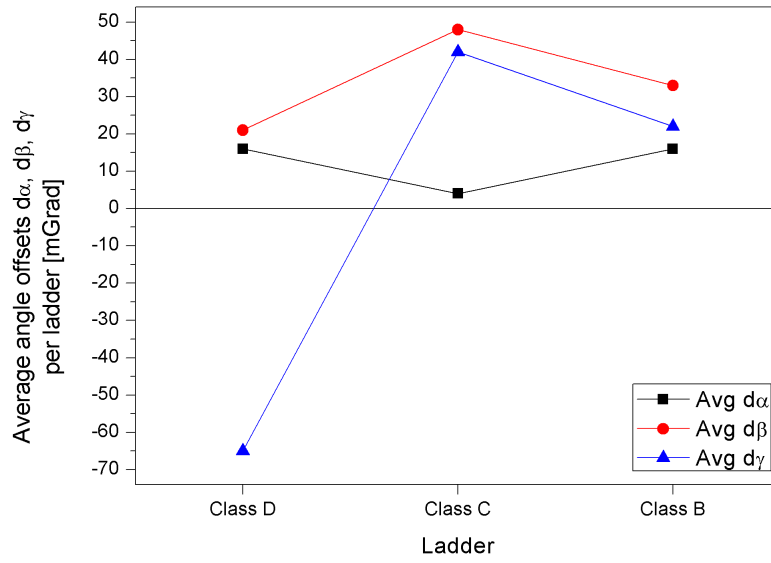


Figure 4.10: Average angle per ladder on class B ladder

The averaged alpha angle offset is very low, but single peak values, as seen in the last section, still remain. The overall alpha angles are close to the positioning uncertainty of the jigs. The beta angle is on average very good as well, but more peak values on different sensors still exist. More tweaking might be necessary here.

5 Outlook

In the current schedule of the Belle II L5 ladder production another class C and another class B ladder is foreseen for assembly until the end of summer 2015. These ladders are made for different testing purposes (e.g. beam tests at CERN or EMC (electromagnetic compatibility) tests in Spain). The ladders will also be used to further improve the mechanical accuracy during assembly. It is expected that the following ladders will show a mechanical accuracy that is consistent with the current class B ladder, or slightly better.

The latest class B ladder showed the currently achievable accuracy. Some adjustments to the jigs are still necessary in order to get a level of mechanical accuracy that is usable for class A ladders. Some gluing and measurement programs will be updated with more automatic features that leaves less error margin for the user.

For the series production, an optimized procedure, which allows jigs and machines to be used in parallel. This enables a quicker production cycle and, even though the jigs are single copies, allows for some of the work to be done in parallel. This could allow the assembly of a full class A ladder to be done in 10 to 12 days including mechanical measurements.

The production of class A ladders, which will be used for the real Belle II detector, will start in Q4 of 2015. This is the so called series production of up to 17 L5 ladders, which will take several months to build. Since the final components are limited, there is almost no margin for errors during the production of class A ladders. Therefore it is essential to acquire the skills that are needed to reach the accuracy levels beforehand.

Bibliography

- [1] Aukom. *Ausbildung Koordinatenmesstechnik e. V.* URL: <http://www.aukom.info/e-learning.html> (visited on 03/09/2015).
- [2] *Belle 2 Technical Design Report*. High Energy Accelerator Research Organization, KEK, 2010.
- [3] Yinon Bendor. *Periodic table*. URL: <http://www.chemicalelements.com/elements/ni.html> (visited on 05/09/2015).
- [4] Thomas Bergauer. *Silicon Detectors in High Energy Physics*. HEPHY, Vienna. URL: <http://www.hephy.at/forschung/alle/vortraege/> (visited on 05/05/2015).
- [5] Sylvie Braibant, Giorgio Giacomelli, and Maurizio Spurio. “Particles and Fundamental Interactions: An Introduction to Particle Physics”. In: 2012th ed. Springer, pp. 11–12.
- [6] CERN. *How a detector works*. URL: <http://home.web.cern.ch/about/how-detector-works> (visited on 02/13/2015).
- [7] Belle Collaboration. *Official Belle Website*. URL: <http://belle.kek.jp/> (visited on 02/24/2015).
- [8] Belle II Collaboration. *The Belle II Silicon Vertex Detector*. HEPHY (Vienna), KEK (Tsukuba), Tohoku University (Sendai).
- [9] The Belle Collaboration. *Physics achievements from the Belle experiment*. Prog. Theor. Exp. Phys. 2012, 04D001. 2012. DOI: [10.1093/ptep/pts072](https://doi.org/10.1093/ptep/pts072).
- [10] Wolfgang Demtröder. “Experimentalphysik 4”. In: 3rd. Springer, pp. 87–88.
- [11] Toni Feder. *Accelerator school travels university circuit*. Physics Today, Feb. 2010. URL: <http://controls.als.lbl.gov/> (visited on 05/05/2015).
- [12] Y. Funakoshi. *SuperKEKB project in detail. Pushing Luminosity of e^-e^+ colliders : The SuperKEKB project*. High Energy Accelerator Research Organization, KEK.
- [13] Jonathan Harris. *Wirebonding Tutorial*. CMC Laboratories, Inc., 2014. URL: <http://www.cmclaboratories.com/documents/> (visited on 03/13/2015).

- [14] Heidenhain. *Encoders for Linear Motors in the Electronics Industry*. URL: http://www.heidenhain.de/de_EN/php/documentation-information/brochures/popup/media/media/file/view/file-0249/file.pdf (visited on 03/09/2015).
- [15] Heidenhain. *Measurement and Control Technology for Demanding Positioning Tasks*. URL: <http://content.heidenhain.de/presentation/basics/de/index/1242135142227/1242135142229/1242135142229.html> (visited on 03/09/2015).
- [16] Heraeus. *Factsheet AlSi*. URL: http://heraeus-contactmaterials.com/media/webmedia_local/media/downloads/documentsbw/factsheets_bw_2012/Factsheet_AlSi_2012.pdf (visited on 05/09/2015).
- [17] KEK High Energy Accelerator Research Organization. URL: www.kek.jp (visited on 02/14/2015).
- [18] AmCraft Manufacturing Inc. *Ultrasonic Welding Technique*. 2015. URL: <http://www.amcrafterfwelding.com/ultrasonic-welding-technique/> (visited on 03/14/2015).
- [19] *KEKB Design Report*. High Energy Accelerator Research Organization, KEK, 2005. URL: <http://www-acc.kek.jp/kekb/publication/> (visited on 02/14/2015).
- [20] Makoto Kobayashi and Toshihide Maskawa. *CP-Violation in the Renormalizable Theory of Weak Interaction*. Kyoto University, Department of Physics, Kyoto, 1972. URL: <http://ptp.oxfordjournals.org/content/49/2/652> (visited on 02/24/2015).
- [21] Manfred Krammer. *Lecture Notes Silicon Detectors*. HEPHY, Vienna, 2011. URL: <http://www.hephy.at/project/halbleiter/VOSkriptum/> (visited on 05/06/2015).
- [22] S. Kurokawa and E. Kikutani. *Overview of the KEKB accelerators*. High Energy Accelerator Research Organization, KEK, 2003. URL: <http://sabotin.ung.si/~sstanic/belle/nim/kekb/NIMA499-1.pdf> (visited on 02/14/2015).
- [23] *Letter of Intent for KEK Super B Factory*. High Energy Accelerator Research Organization, KEK. Chap. Part 3: Accelerator Design.
- [24] Valentin M. “The Silicon Vertex Detector for b-tagging at Belle II”. Dissertation. Institute for High Energy Physics, Vienna, 2013.
- [25] Yuki Yoshi Ohnishi. *Accelerator design at the SuperKEKB*. Prog. Theor. Exp. Phys. 2013, 03A011. High Energy Accelerator Research Organization, KEK. DOI: [10.1093/ptep/pts083](https://doi.org/10.1093/ptep/pts083).
- [26] Lexikon der Physik. *Paarbildung*. URL: <http://www.spektrum.de/lexikon/physik/paarbildung/10835> (visited on 02/14/2015).

Bibliography

- [27] Renishaw. *Touch-trigger probe systems User Guide*. URL: <https://www.renishaw.com/cmmsupport/knowledgebase/en/14271.aspx> (visited on 01/20/2015).
- [28] Schultschik Stefan. “High precision gluing and measurement methods for the Belle 2 silicon vertex detector”. Project work. Institute for High Energy Physics, Vienna.